Journal of Nuclear Medicine, published on April 9, 2021 as doi:10.2967/jnumed.121.261977

Title: Improved Radium-223 Therapy with Combination Epithelial Sodium Channel Blockade

Authors: Diane S. Abou, Ph.D.[1,2,3], Amanda Fears, B.S.[1], Lucy Summer, B.S.[1], Mark Longtine, Ph.D.[1], Nadia Benabdallah, Ph.D.[1,2], Ryan C. Riddle, Ph.D.[4,5], David Ulmert, M.D., Ph.D.[6,7], Jeff M. Michalski, M.D., M.B.A., F.A.S.T.R.O.[8], Richard L. Wahl, M.D.[1], Denise Chesner, B.S.[9], Michele Doucet, B.S.[10], Nicholas C. Zachos, Ph.D.[9], Brian W. Simons, Ph.D.[11], Daniel L. J. Thorek, PhD[1,2,3,12]

Affiliations:

1 Mallinckrodt Institute of Radiology, Washington University in St. Louis, School of Medicine, St. Louis, Missouri, 63110
2 Program in Quantitative Molecular Therapeutics, Washington University in St. Louis, School of Medicine, St. Louis, Missouri, 63110
3 Cyclotron Facility, Washington University in St. Louis, School of Medicine, St. Louis, Missouri, 63110
4 Department of Orthopaedics, Johns Hopkins University, Baltimore, Maryland, 21205
5 Research and Development Service, Baltimore VA Medical Center, Baltimore, MD 21201
6 Department of Pharmacology, University of California Los Angeles, Los Angeles, California, 90032
7 Department of Clinical Sciences, Lund University, Barngatan 2:1, Lund, S-21185 Sweden
8 Department of Radiation Oncology, Washington University in St. Louis, School of Medicine, St. Louis, Missouri, 63110
9 Department of Medicine, Division of Gastroenterology and Hepatology, Johns Hopkins University, School of Medicine, Baltimore, Maryland, 21225
10 Department of Oncology, Johns Hopkins University, School of Medicine, Baltimore, Maryland, 21225
11 Center for Comparative Medicine, Baylor College of Medicine, Houston, Texas, 77030.
12 Department of Biomedical Engineering, Washington University in St. Louis, St. Louis, Missouri, 63110

Corresponding Author:

Daniel LJ Thorek
Department of Radiology, Washington University in St. Louis,
510 S. Kingshighway Blvd. St. Louis, Missouri, 63110
314-747-5624 | thorekd@wustl.edu

ABSTRACT

Background: Radium-223 dichloride ([^{223}Ra]$RaCl_2$) is the first approved alpha particle-emitting therapy and is indicated for treatment of bone metastatic castrate resistant prostate cancer. Approximately half of the dose is absorbed into the gastrointestinal (GI) tract within minutes of administration, limiting disease-site uptake and contributing to toxicity. Here, we investigate the role of enteric ion channels and their modulation for improved therapeutic efficacy and reduced side effects.

Methods: Utilizing primary human duodenal organoids (enteroids) as *in vitro* models of the functional GI epithelium, we found that Amiloride (ENaC blocker) and NS-1619 (K^+ channel activator) presented significant effects in ^{223}Ra membranal transport. Radioactive drug distribution was evaluated for lead combinations *in vivo*, and in osteosarcoma and prostate cancer models.

Results: Amiloride shifted ^{223}Ra uptake in vivo from the gut, to nearly double the uptake at sites of bone remodeling. Bone tumor growth inhibition with the combination as measured by bioluminescent and X-ray imaging was significantly greater than single agents alone, and the combination resulted in no weight loss.

Conclusion: This combination of approved agents may be readily implemented as a clinical approach to improve outcomes of bone metastatic cancer patients with the benefit of ameliorated tolerability.

Key words: Radium-223, amiloride, ion channel, gastro-intestinal, bone

Running title: Modifying Radium-223 Distribution

INTRODUCTION

Prostate adenocarcinoma is the most common non-cutaneous cancer diagnosed in men. Early treatment with radiation or surgery has a high rate of success, however recurrent disease is incurable. Prostate cancer (PCa) frequently metastasizes to the bone, where physical and microenvironmental factors make both focal and systemic treatments less effective. Bone metastases cause debilitating pain, fracture, and displace the hematological compartment and ultimately death (*1*,*2*).

In 2013 Radium dichloride ($[^{223}Ra]RaCl_2$) became the first approved therapy specifically for improved survival in men with castrate-resistant PCa bone metastases. This first-in-class alpha particle (α) emitting therapy has a manageable haematological profile, significantly delays symptomatic skeletal events and extends overall survival in line with next-generation antiandrogens (*3*,*4*). α's deposit MeV of energy to cells adjacent the site of decay. Localizing to sites of bone turnover apposite skeletal metastases, the relative biological effect of ^{223}Ra is several fold conventional external beam radiation, and treatment is not limited by factors such as hypoxia (*5*).

Despite the ablative potential of α-therapy, survival improvements are modest. This may be due in part to insufficient delivery of radioisotope as well as dose limitations for its safe application. Radium is an alkaline earth metal that accumulates at sites of bone turnover; however nearly half of the administered activity accumulates within minutes in the GI (*6*,*7*). This reduces the activity reaching sites of disease and is associated with radiotoxic sequalae in the GI from ^{223}Ra and daughters' decay (*8*). While GI disposal is known (*9*,*10*), the biological basis for transport of ^{223}Ra from the blood to the lumen has not been investigated and the overwhelming majority of metal-transport literature concerns apical-to-basolateral absorption.

Investigations of ^{223}Ra clearance in small animals recapitulates that found in man, with >50% of the initial activity cleared by 24 h (*11–13*). In this work, we evaluate radium ion transport to the gut following intravenous administration and the impact of pharmacophores to modulate this flux. Using *in vitro* enteric systems and *in vivo* evaluation of organ distribution, we show GI uptake can be inhibited by amiloride, a clinically approved epithelial sodium ion channel (ENaC) blocker. When used in combination, ^{223}Ra is rerouted from radiosensitive organs to sites of active bone turnover at metastases providing therapeutic benefit in a PCa model of bone metastasis and

reduced treatment-induced toxicity. These data motivate clinical evaluation of this approach for improved α-therapy.

MATERIALS AND METHODS

Chemicals and Isotope Production

Chemicals were purchased from Sigma-Aldrich, unless otherwise noted. [^{223}Ra]$RaCl_2$ was produced as previously described method (*14*) wherein pure ^{223}Ra was generated from the parent isotope ^{227}Th or ^{227}Ac source provided by Oak Ridge National Laboratory, Department of Energy. Briefly, 10-20 μCi of parent isotope was adsorbed on an anionic polymeric resin Dowex 1x8 and eluted under mild acidic conditions (methanol: nitric acid (2 N) 80:20) to isolate ^{223}Ra-nitrates. The final sample was suspended in sodium citrate (0.03 M) and saline (150 mM) and assessed by high purity germanium detector, showing undetectable isotopic parent breakthrough and a ^{223}Ra radiochemical purity of over 99%.

In vitro studies

Cultured human duodenal enteroids and Caco-2/BBe1 monolayers were grown on Transwell polymeric filters. This permitted quantification of ^{223}Ra transcellular transport, mimicking the physiological excretion of ^{223}Ra. Monolayer growth conditions, integrity tests and counting methodology are detailed in Supplemental Information (*15–17*).

In vivo studies

Animal experiments were conducted in accordance with Institutional Animal Care and Use Committee approved protocols of the Johns Hopkins University School of Medicine and Washington University School of Medicine (*18*).

Autoradiography

Aged male C57Bl/6 mice (>35 wk) were retro-orbitally administered 250 kBq/kg [^{223}Ra]$RaCl_2$ and sacrificed at 10 min; 1; 4; 24; 48 h. The whole GI tract from stomach to rectum was rapidly harvested and placed on cellophane (approximately 35 μm thickness) set over autoradiographic phosphor screens for 90 min exposure, protected from light, and read on Cyclone Phosphor Imager (Packard) at 300 DPI (*19*).

Immunohistological staining

Male C57Bl/6 mice (Charles River) aged 20-30 weeks old were treated with Golytely (24g/350mL) 2 h prior to intravenous [^{223}Ra]$RaCl_2$ (250 kBq/kg). Portions (1 cm) of duodenum, jejunum, ileum and colon were harvested at 24 h, embedded in O.C.T. and flash frozen. Transversal sectioning was conducted utilizing Leica 1860 cryomicrotome at 10 μm, fixed by immersion in 10% paraformaldehyde (15 min). Stained slides (Supplemental Information) were mounted using DAPI and/or TRITC-Phalloidin media and imaged (Zeiss Axioplan M1 μmanager 2.0) (*20*).

Radioactive organ distribution

Male C57Bl/6 mice aged >12 weeks (n=6) were dosed intraperitoneally with Amiloride (12.5 mg/kg -150 μL 2%v/v DMSO) or NS-1619 (1mg/kg – 150 μL 2% v/v DMSO) 1 h prior to retro-orbital [^{223}Ra]$RaCl_2$ injection (3.7 KBq in 100 μL citrate saline buffer). Tissues were harvested at 15 min; 1; 4; 24; 48; 240 h post-administration of radionuclide, weighed and gamma counted with an energy range of 150-350 KeV, 10 min per sample (Wizard2, Perkin Elmer). Standard samples (10 % of injected activity) were measured, and percent injected (%IA) normalized to tissue weight (%IA/g) reported. Dosimetry was computed from these data, as detailed in Supplemental Information (*21–23*).

Tumor distribution, response and toxicity studies

Male Rag2-Il2rg double knockout mice mice >12 wks (R2G2; Envigo) were implanted with 5E6 Saos-2 osteosarcoma cells in the flank, or with 2.5E5 luciferase expressing C4-2B cells in the tibia (*24*). Animals were

monitored by planar X-ray (MX20, Hologic) and bioluminescence imaging (BLI; IVIS, Perkin Elmer) for xenograft progression and response. For uptake in the osteosarcoma model mice were divided into two cohorts for [^{223}Ra]$RaCl_2$ injection alone or with amiloride, as above. For C4-2B bone metastasis treatment, animals were randomized to receive amiloride or [^{223}Ra]$RaCl_2$ alone or the combination. For toxicological studies, male FVB/NCR aged 14 wks (n=5) were randomized into 4 cohorts treated with 1) [^{223}Ra]$RaCl_2$ alone (3.7 KBq/100 μL); or 2) amiloride alone (12.5 mg/kg i.p.); or 3) combination amiloride with [^{223}Ra]$RaCl_2$ or 4) control untreated (saline). Weight change and blood chemistry analysis was monitored for 20d and histopathology assessment by a certified veterinary pathologist. Treatment, imaging and procedural details are found in Supplemental Information.

Statistics

Significance was calculated with unpaired two-tailed t-test with equal standard deviation (SD), utilizing Graphpad (version 6D). Significant differences were expressed at $P<0.05$ and $P<0.1$.

RESULTS

Gastrointestinal Accumulation and Transit of ^{223}Ra

It has been established that preclinical models accurately reflect the clinical distribution and kinetics of $^{223}RaCl_2$ following intravenous administration (*11–13*,*24*,*25*). A majority of activity is transferred from circulation into the small intestine within minutes. To study the kinetics of elimination, we performed whole organ autoradiography of the murine GI at various times (10 min to 48 h) after administration of 55 kBq/kg of [^{223}Ra]$RaCl_2$ (Figure 1A).

Activity was detected at a high level as early as 10 min in the distal stomach and duodenum (Figure 1A,B). Radium and daughters were then passed for nearly complete clearance by 24 h. Immunofluorescence revealed radiobiological damage generated by ^{223}Ra transit (Figure 1C). Tissue morphology was displayed using DAPI (4,6-diamidino-2-phenylindole) and phalloidin, with DNA damage, cell apoptosis and proliferation assessed using markers for γH_2AX, TUNEL (terminal deoxynucleotidyl transferase dUTP nick end labeling) and

Ki67 at 4 and 24 h (Supplemental Figure 1). Radiation-related damage was identified in the duodenum and colon at 24 h, correlating with clearance kinetics.

In Vitro Assessment of Active ^{223}Ra Transport

Transport from the basolateral to apical (luminal) compartment across human primary duodenal enteroid monolayers was used to model the blood and intestinal compartments (Figure 2A). We first tested if ^{223}Ra transport was an active or passive process at physiological and reduced temperatures (Figure 2B). As expected, flux was suppressed at lower temperature, in agreement with an active mechanism.

Location and maturation stage of enterocytes present characteristic ion channel profiles (*16*). Using undifferentiated (immature crypt-like enterocytes) and differentiated (mature villi-like brush border enterocytes) enteroids grown from patient biopsies, we observed a significant preference for ^{223}Ra transport across differentiated monolayers 2.2±0.3 % over undifferentiated 1.6±0.2 % (P<0.05; Figure 2C). The active and cell-type specific ^{223}Ra transport led us to evaluate modulators to influence this flux.

Caco-2 cells in a microtranswell system were screened with 52 ion channel modulators incubated with [^{223}Ra]$RaCl_2$. Monolayer integrity was ensured by resistance and control-fluorescent compound measures. 40 molecules increased flux as compared to control, and 11 drugs inhibited transfer. The K^+ channel activator NS-1619 was among the most effective in increasing ^{223}Ra transport up to 3.3±1.6 fold (*26*). In contrast, amiloride, an approved diuretic Na^+/H^+ channel blocker decreased ^{223}Ra transfer to 0.70±0.14 fold. Despite electrochemical similarities, calcium channel blockers were ineffective ^{223}Ra-inhibitors.

Modulation of ^{223}Ra Distribution

The pharmacokinetic impact on ^{223}Ra by lead compounds to either promote (1 mg/kg NS-1619) or inhibit (12.5 mg/kg amiloride) enteric transit were assessed by biodistribution. Ion channel modulation is transient (*27*,*28*), and an initial dose and schedule-finding study was performed (Supplemental Information and Supplemental Figures 2 and 3). Organ activity levels from skeletally mature animals are shown as %IA/g (Figure 3A and Supplemental Table 1). Increasing amounts of activity in the bone following radiopharmaceutical

administration are accompanied by kidney and upper GI uptake (stomach, duodenum and jejunum), which is passed (Figure 1A).

Intestinal absorption was significantly greater at early time points: stomach uptake at 15 min of 2.73±0.44 %IA/g with NS-1619 was 2-fold over control (1.39±0.6%) with a concomitant decrease in osseous uptake (P<0.05; Figure 3A,B). In contrast, the amiloride combination decreased GI and renal uptake of ^{223}Ra, and delayed kinetics of transport through the GI. Upper GI uptake was lower than that of the control and ion channel activator combination at 15 min (%IA) with greater ^{223}Ra in the tibia, reaching 22.62 ± 3.62 over that of control level of 13.96 ± 4.32 %IA/g (P<0.05).

We evaluated changes beyond the acute setting out to the physical half-life of the radionuclide (Figure 3C,D and Supplemental Table 2). Bone uptake for the combination with amiloride at 18.9 ± 8.3 %IA/g was nearly twice that of the control group 10.2 ± 5.4 %IA/g at 48 h. Dynamic turnover reduced activity to nearly equal 10 %IA/g at 10 d (Supplemental Figure 4). Estimating absorbed doses at the organ scale, we measured a significant increase in therapeutic energy deposition at the intended osseous sites 1.43 Gy, compared to 1.03 Gy for [^{223}Ra]$RaCl_2$ only treatment (Supplemental Information).

Bone Tumor Targeting and Therapeutic Outcomes

Quantification of radionuclide localization in rodent models of bone metastasis is complicated by continued normal bone turnover, as the epiphyseal plates of mice do not fuse (*13*). To address this, we tested heterotopic ossification using an osteosarcoma model. Mineralized subcutaneous tumor were identified using X-ray and [^{18}F]NaF PET (Figure 4). Tissues of interest were excised, counted and weighed at 24 h following [^{223}Ra]$RaCl_2$ (55 kBq/kg) with or without combination amiloride (12.5 mg/kg). At this time point, no difference in kidney or GI uptake was noted, however tibia (P<0.005) and osteosarcoma (P<0.01) samples from the combination treatment have increased ^{223}Ra accumulation (Supplemental Figure 5).

An intratibial inoculation of luciferase-expressing castrate resistant C4-2B cells (*29*) was used to test impact in the therapeutic setting by BLI and X-ray imaging (Supplemental Figure 6). Animals were randomized to receive 1) [^{223}Ra]$RaCl_2$ alone; 2) [^{223}Ra]$RaCl_2$ in combination with amiloride; or 3) Amiloride alone.

Approximately 30-fold increase of radiance was observed for the amiloride only group at 33 days post-treatment, indicating no anti-tumor effect for the mixed osteolytic/blastic C4-2B lesions (Figure 4 and Supplemental Figure 6). Body mass was monitored and shows that the combination resulted in less weight loss, as well as more rapid regain rate. These data show both disease burden reduction and sparing of GI from the transient initial dose enables faster recovery. At termination, radiographs display reduced osteolysis due to combination treatment.

Toxicological Evaluation of Combination

To investigate potential combination induced sequelae, we randomized mice into four cohorts to receive saline, amiloride, [^{223}Ra]$RaCl_2$ or the combination. Clinical chemistry analysis was conducted using a multiparameter blood panel over 19 d. Post-mortem kidney tissues underwent histopathology to identify potential treatment related damage, and weight was monitored throughout (Figure 5). The majority of clinical chemistry values across all cohorts did not deviate significantly from vehicle. Levels of alkaline phosphatase (ALP) and creatinine (CRT) were decreased for both Radium-treatment groups at day 7 (CRT: 11-14 μmol/L; ALP: 47-51 u/L) as compared to vehicle (CRT: 16 μmol/L; ALP: 66.7 u/L). CRT recovered to control level values after 7 days, while ALP remained suppressed. This may reflect clinical experience with patients on [^{223}Ra]$RaCl_2$ (*30*,*31*).

The slight increase in renal excretion of ^{223}Ra measured from the combination at 4 h p.i. (Figure 3A,B) led us to investigate kidney status by standard histopathology. Morphological analysis of tissue sections by H&E and Periodic acid-Schiff (PAS), as well as renal fibrosis (Masson's trichrome) indicated no aberrant pathology across groups at 20 d. Additionally, all animals put on weight without significant difference (Figure 5C).

DISCUSSION

After decades of development in the field of targeted nuclear therapy, [^{223}Ra]$RaCl_2$ became the first EMA/FDA approved α-therapy in 2013 (*32*). This treatment improves survival, reduces fracture incidence and decreases bone pain in men with bone metastatic PCa. While well tolerated, responses are moderate and ^{223}Ra and its daughters' sequestration in the GI can result in treatment cessation (*8*), and reduces dose to disease sites.

Radium research has focused on bone and metastases (*11*,*24*,*33–35*). As a starting point to assess the distribution of [^{223}Ra]$RaCl_2$ we validated of preclinical models to approximate human clearance (*6*). Our work in skeletally mature mice recapitulates ^{223}Ra distribution in man (*11–13*) and whole tract imaging of excised GI show pharmacokinetics similar to that of patients, with uptake in stomach and duodenum as early as 10 min p.i. (Figure 1). Immunofluorescence revealed radiation damage at the cellular level associated with cellular apoptosis and DNA damage activity. Specifically, γH2AX signal of the duodenum and colon localized at the apical surface of the lumen matching our visualization of the clearance.

The kinetics of this phenomenon led us to hypothesize that active cellular processes mediated by ion transport are involved, and further that pharmacological modulation may decrease toxicity and improve therapeutic outcomes. Radium is an alkaline earth metal yet its transport was not altered by Ca^{2+} channel blockers. Verapamil, a prototypical calcium channel inhibitor, had little effect *in vitro,* or *in vivo* (Supplemental Figure 7). Instead, Na^+/H^+ channel modulators such as amiloride and benzamil had potent inhibitory effects and did not disturb enteroid integrity. Fipronil showed even greater efficacy in ^{223}Ra blockade, however this insecticide was excluded from further study. Diverse families of ion channels are expressed throughout the GI, regulating critical functions of nutrient and fluid secretion and absorption, and motility. The modulators tested affect different families of ion channels and do not confirm an exclusive ^{223}Ra-dependent transporter or class, and identification of specific ^{223}Ra-transport channels requires further investigation.

In vivo data of lead compounds confirmed cellular assay results (Figure 3). Study parameters were determined from a dose and timing study demonstrating intraperitoneal of amiloride 1 h prior to [^{223}Ra]$RaCl_2$, at a dose of 12.5 mg/kg, robustly inhibited intestinal transport and increased bone accumulation (Supplemental Figures 3 and 4). Further optimization for other combinations may be required. Amiloride combined with [^{223}Ra]$RaCl_2$ transiently decreased GI accumulation and drove a substantial increase to bone (nearly two-fold). In contrast, NS-1619 increased acute upper GI sequestration. Increased uptake in the skeleton with the Radium and amiloride combination results in a greater total energy deposited (Supplemental Table 3).

These results encouraged us to pursue the amiloride with [^{223}Ra]$RaCl_2$ in the disease setting after first confirming the osteoid targeting properties of the combination in an osteosarcoma model of pathological bone. A

significantly decreased bone tumor burden in the ^{223}Ra cohorts was observed, with more rapid and deeper response in the combination cohort. These outcomes, following a single administration, were accompanied by faster renormalization of weight and we presume recovery is due to decreased tumor burden and mitigated gastrointestinal damage. Clinical chemistry and histopathology were also carried out showing creatinine values followed the trend of regained weight. Amiloride side effects include dizziness, muscle spasms and nausea; and patients with impaired renal function will need to be closely monitored.

These results are impactful for radium patients as many men bear substantial disease; have faced several prior lines of potentially toxic cancer therapy; and have comorbidities engendering careful patient management. We anticipate that the increased tolerability and dose accumulation at sites of disease are likely to synergize over the course of the 6 cycles to extend both treatment duration and magnitude of response.

CONCLUSION

Investigations using cellular systems and *in vivo* models demonstrate that ^{223}Ra uptake is an active cellular process. The novel combination of amiloride with [^{223}Ra]$RaCl_2$ improved efficacy of α-therapy. The attendant reduction in absorbed dose to other sites ameliorated tolerability issues and was found to minimally impact at-risk organs or clinical chemistry profiles. This combination of two approved agents warrants further evaluation in the patient management setting.

DISCLOSURES

The authors declare no conflict of interest.

ACKNOWLEDGEMENTS

SNMMI Junior Faculty Fund 2015 (DSA); the Patrick C. Walsh Prostate Cancer Research Fund (DLJT); the National Cancer Institute R01CA229893 (DLJT), R01CA201035 (DLJT) and R01CA240711 (DLJT). We thank Dr. Slusher of JHU for Topcount use and acknowledge the Integrated Physiology Core of the Hopkins Conte Digestive Disease Basic and Translational Research Core Center P30DK-089502 (NCZ) for human enteroids and media.

KEY POINTS

QUESTION: We asked if it is possible to inhibit the rapid uptake of ^{223}Ra in the gastrointestinal tract in order to drive greater dose to bone metastases.

PERTINENT FINDINGS: Amiloride combined with [^{223}Ra]$RaCl_2$ decreased GI accumulation and resulted in a substantial increase (nearly two-fold) in bone uptake. The combination improved efficacy of therapy to delay metastatic growth while presenting no apparent toxicity.

IMPLICATION FOR PATIENT CARE: This novel strategy has significant potential to improve on-target ^{223}Ra effect at the same time as reducing treatment induced toxicities and weight loss.

REFERENCES

1. Siegel RL, Miller KD, Jemal A. Cancer statistics, 2020. *CA Cancer J Clin*. 2020;70:7-30.

2. Printz C. Prostate cancer mortality projections reach a new high: With prostate cancer deaths projected to rise to their highest level in 20 years, some experts worry that changes to screening guidelines made in 2012 could be a factor. *Cancer*. 2020;126:3893-3894.

3. Sartor O, Coleman R, Nilsson S, et al. Effect of radium-223 dichloride on symptomatic skeletal events in patients with castration-resistant prostate cancer and bone metastases: results from a phase 3, double-blind, randomised trial. *Lancet Oncol*. 2014;15:738-746.

4. Parker C, Nilsson S, Heinrich D, et al. Alpha emitter radium-223 and survival in metastatic prostate cancer. *N Engl J Med*. 2013;369:213-223.

5. Baidoo KE, Yong K, Brechbiel MW. Molecular pathways: targeted α-particle radiation therapy. *Clin Cancer Res*. 2013;19:530-537.

6. Carrasquillo JA, O'Donoghue JA, Pandit-Taskar N, et al. Phase I pharmacokinetic and biodistribution study with escalating doses of ^{223}Ra-dichloride in men with castration-resistant metastatic prostate cancer. *Eur J Nucl Med Mol Imaging*. 2013;40:1384-1393.

7. Flux GD. Imaging and dosimetry for radium-223: the potential for personalized treatment. *Br J Radiol*. 2017;90:20160748.

8. Jadvar H, Challa S, Quinn DI, Conti PS. One-Year Postapproval Clinical Experience with Radium-223 Dichloride in Patients with Metastatic Castrate-Resistant Prostate Cancer. *Cancer Biother Radiopharm*. 2015;30:195-199.

9. Harrison GE, Carr TE, Sutton A, Rundo J. Plasma concentration and excretion of calcium-47, strontium-85, barium-133 and radium-223 following successive intravenous doses to a healthy man. *Nature*. 1966;209:526-527.

10. Harrison GE, Carr TE, Sutton A. Distribution of radioactive calcium, strontium, barium and radium following intravenous injection into a healthy man. *Int J Radiat Biol Relat Stud Phys Chem Med*. 1967;13:235-247.

11. Abou DS, Ulmert D, Doucet M, Hobbs RF, Riddle RC, Thorek DLJ. Whole-Body and Microenvironmental Localization of Radium-223 in Naïve and Mouse Models of Prostate Cancer Metastasis. *J Natl Cancer Inst*. 2016;108.

12. Abou DS, Rittenbach A, Tomlinson RE, et al. Preclinical Single Photon Emission Computed Tomography of Alpha Particle-Emitting Radium-223. *Cancer Biother Radiopharm*. March 2020.

13. Jiang W, Ulmert D, Simons BW, Abou DS, Thorek DLJ. The impact of age on radium-223 distribution and an evaluation of molecular imaging surrogates. *Nucl Med Biol*. 2018;62-63:1-8.

14. Abou DS, Pickett J, Mattson JE, Thorek DLJ. A Radium-223 microgenerator from cyclotron-produced trace Actinium-227. *Appl Radiat Isot*. 2017;119:36-42.

15. Noel G, Baetz NW, Staab JF, et al. A primary human macrophage-enteroid co-culture model to investigate mucosal gut physiology and host-pathogen interactions. *Sci Rep*. 2017;7:45270.

16. Foulke-Abel J, In J, Yin J, et al. Human enteroids as a model of upper small intestinal ion transport physiology and pathophysiology. *Gastroenterology*. 2016;150:638-649.e8.

17. Foulke-Abel J, In J, Kovbasnjuk O, Zachos NC. Human intestinal enteroids: a new model to study human rotavirus infection, host restriction and pathophysiology. *Journal of*. 2015.

18. Institute for Laboratory Animal Research (U. S.) (U. S.), National Academies Press (U. S. Guide for the care and use of laboratory animals (8th edition). Washington, D.C., DC: National Academies Press; 2011.

19. Schindelin J, Arganda-Carreras I, Frise E, et al. Fiji: an open-source platform for biological-image analysis. *Nat Methods*. 2012;9:676-682.

20. Edelstein AD, Tsuchida MA, Amodaj N, Pinkard H, Vale RD, Stuurman N. Advanced methods of microscope control using μManager software. *J Biol Methods*. 2014;1:10.

21. Bolch WE, Eckerman KF, Sgouros G, Thomas SR. MIRD Pamphlet No. 21: A Generalized Schema for Radiopharmaceutical Dosimetry—Standardization of Nomenclature. *J Nucl Med*. 2009;50:477-484.

22. Miloudi H, Locatelli M, Autret G, et al. Application of rodes software to experimental biokinetic data for dose assessment in mice and rats. *J Radiol Prot*. 2017;37:564-583.

23. Locatelli M, Miloudi H, Autret G, et al. RODES software for dose assessment of rats and mice contaminated with radionuclides. *J Radiol Prot*. 2017;37:214-229.

24. Dondossola E, Casarin S, Paindelli C, et al. Radium 223-mediated zonal cytotoxicity of prostate cancer in bone. *J Natl Cancer Inst*. January 2019.

25. Suominen MI, Fagerlund KM, Rissanen JP, et al. Radium-223 Inhibits Osseous Prostate Cancer Growth by Dual Targeting of Cancer Cells and Bone Microenvironment in Mouse Models. *Clin Cancer Res*. 2017;23:4335-4346.

26. Olesen SP, Munch E, Moldt P, Drejer J. Selective activation of Ca(2+)-dependent K+ channels by novel benzimidazolone. *Eur J Pharmacol*. 1994;251:53-59.

27. Ningaraj NS, Rao M, Hashizume K, Asotra K, Black KL. Regulation of blood-brain tumor barrier permeability by calcium-activated potassium channels. *J Pharmacol Exp Ther*. 2002;301:838-851.

28. Vidt DG. Mechanism of action, pharmacokinetics, adverse effects, and therapeutic uses of amiloride hydrochloride, a new potassium-sparing diuretic. *Pharmacotherapy*. 1981;1:179-187.

29. Thalmann GN, Sikes RA, Wu TT, et al. LNCaP progression model of human prostate cancer: androgen-independence and osseous metastasis. *Prostate*. 2000;44:91-103 Jul 1;44(2).

30. Kuppen MC, Westgeest HM, van der Doelen MJ, et al. Real-world outcomes of radium-223 dichloride for metastatic castration resistant prostate cancer. *Future Oncol*. 2020;16:1371-1384.

31. Sartor O, Coleman RE, Nilsson S, et al. An exploratory analysis of alkaline phosphatase, lactate dehydrogenase, and prostate-specific antigen dynamics in the phase 3 ALSYMPCA trial with radium-223. *Ann Oncol*. 2017;28:1090-1097.

32. Kluetz PG, Pierce W, Maher VE, et al. Radium Ra 223 dichloride injection: U.S. Food and Drug Administration drug approval summary. *Clin Cancer Res*. 2014;20:9-14.

33. Henriksen G, Breistøl K, Bruland ØS, Fodstad Ø, Larsen RH. Significant antitumor effect from bone-seeking, alpha-particle-emitting (223)Ra demonstrated in an experimental skeletal metastases model. *Cancer Res*. 2002;62:3120-3125.

34. Henriksen G, Fisher DR, Roeske JC, Bruland ØS, Larsen RH. Targeting of osseous sites with alpha-emitting 223Ra: comparison with the beta-emitter 89Sr in mice. *J Nucl Med*. 2003;44:252-259.

35. Suominen MI, Rissanen JP, Käkönen R, et al. Survival benefit with radium-223 dichloride in a mouse model of breast cancer bone metastasis. *J Natl Cancer Inst*. 2013;105:908-916.

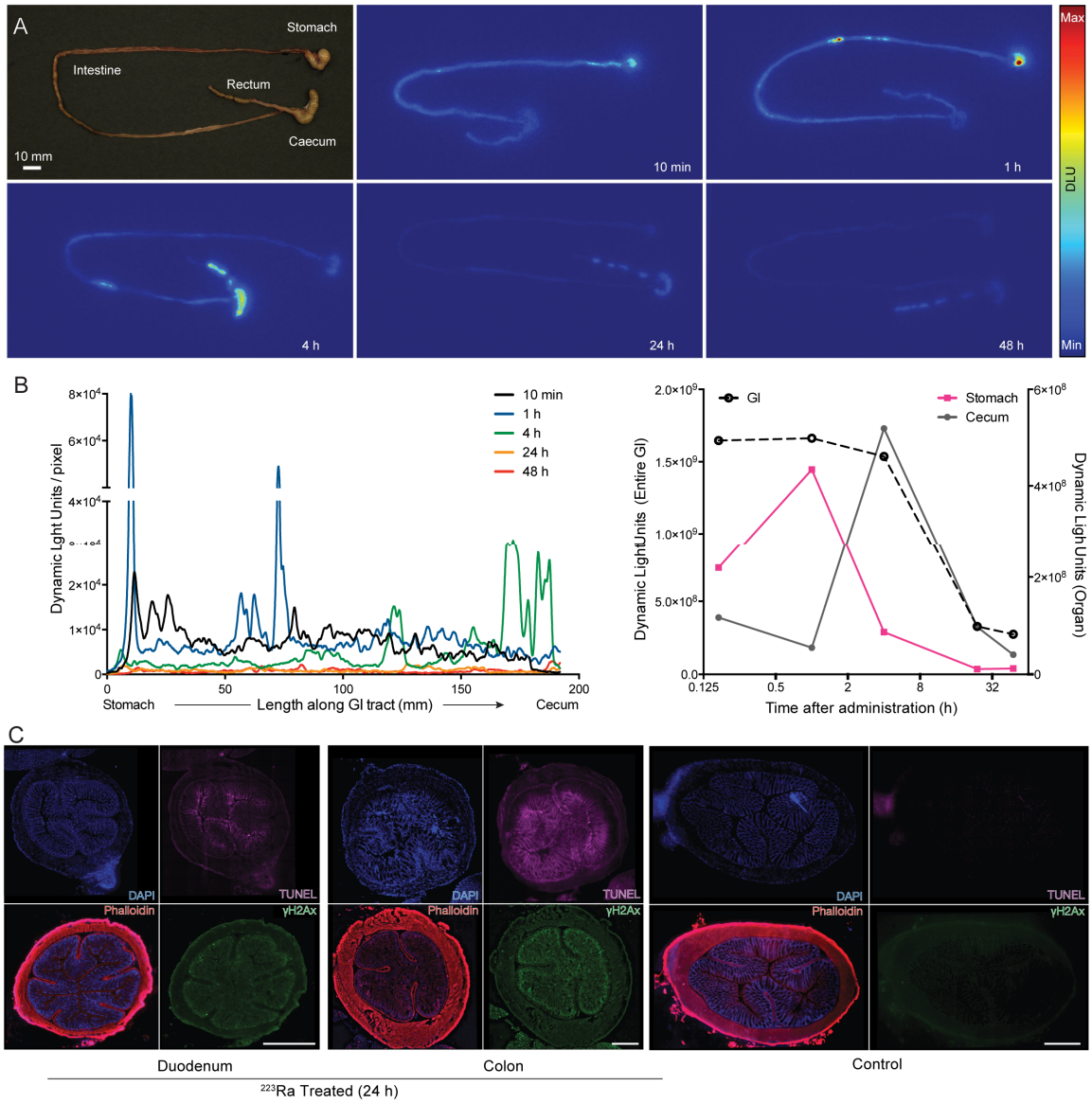

Figure 1: GI transit of [^{223}Ra]$RaCl_2$ and radiobiological effects. A) Radium-223 dichloride autoradiography of the mouse GI. B) Signal intensity profiles from stomach to cecum displaying the isotope migration (approximately 200 mm/animal) at indicated time points. Upper (stomach), lower (cecum) compartments and complete organ signal quantification, over time. C) Immunofluorescence of duodenum and colon sections following treatment (left) and colonic section of saline control mouse (right). For each micrograph the stain and color is indicated; DAPI for nuclei, phalloidin for cytoskeleton, the TUNEL marker for apoptosis and γ-H2AX for DNA damage.

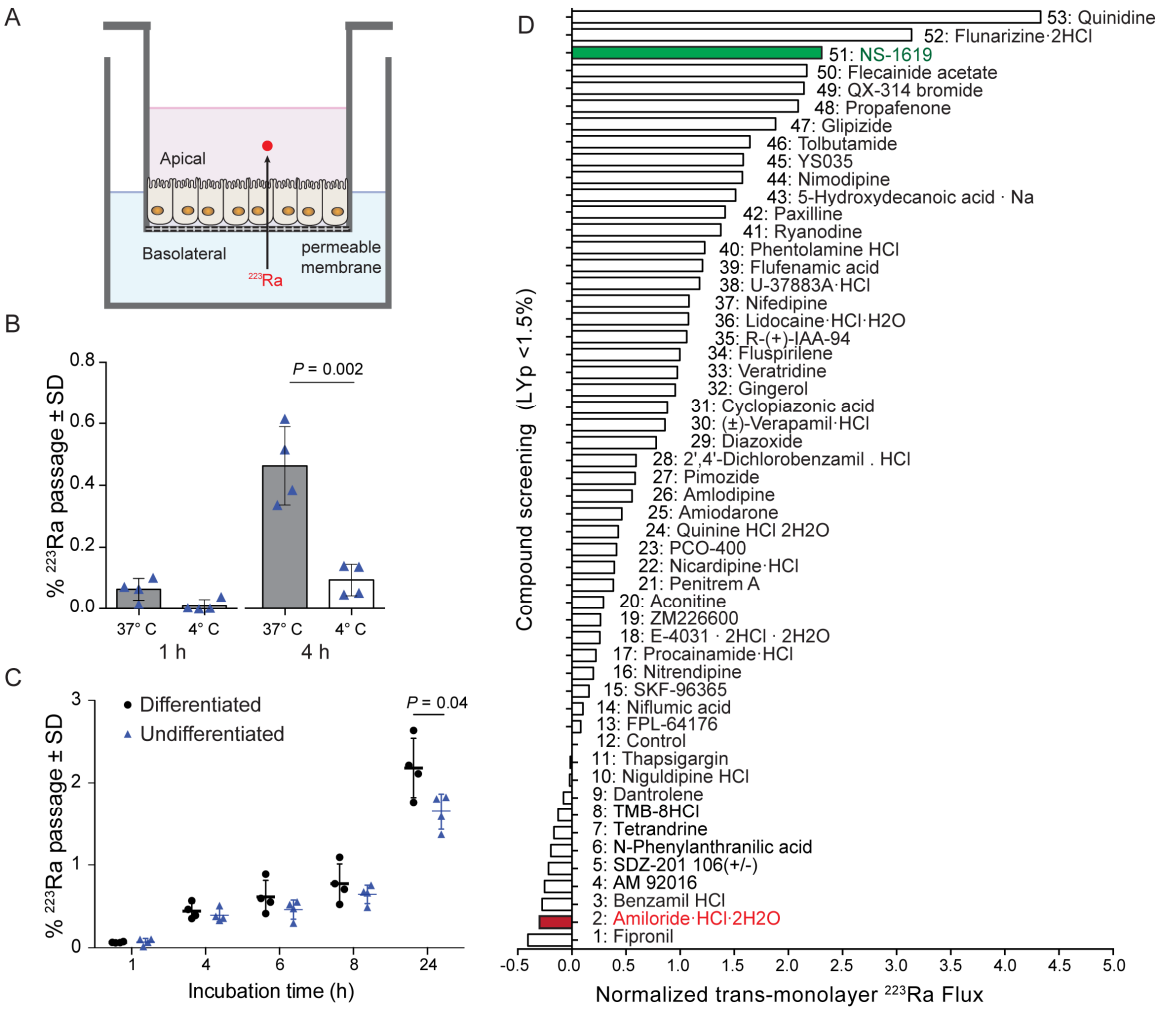

Figure 2: Active Radium-223 transport through human gastrointestinal organoids; A) Schematic representation of enteroid monolayers grown on a permeable transwell. B) Radium-223 passage to the apical compartment normalized to the initial dose in the basolateral media reveal temperature-dependent mechanism, with undifferentiated crypt-like enteroids. C) Increased ^{223}Ra transport measured using differentiated over undifferentiated enteroids as a function of time (P<0.05). D) ^{223}Ra flux normalized to untreated well was measured through caco-2 monolayers co-incubated with a library of 52 ion-channel inhibitors or activators. Caco-2 monolayer integrity was confirmed by pre- and post-radioactive incubation measuring TEER and Lucifer yellow (LyP < 1.5%) readings. The average differential of radioactive counts (n=3) has been normalized to ^{223}Ra flux baseline exempt of treatment (#12 control well). Amiloride (red) and NS-1619 (green) proceeded for *in vivo* validation.

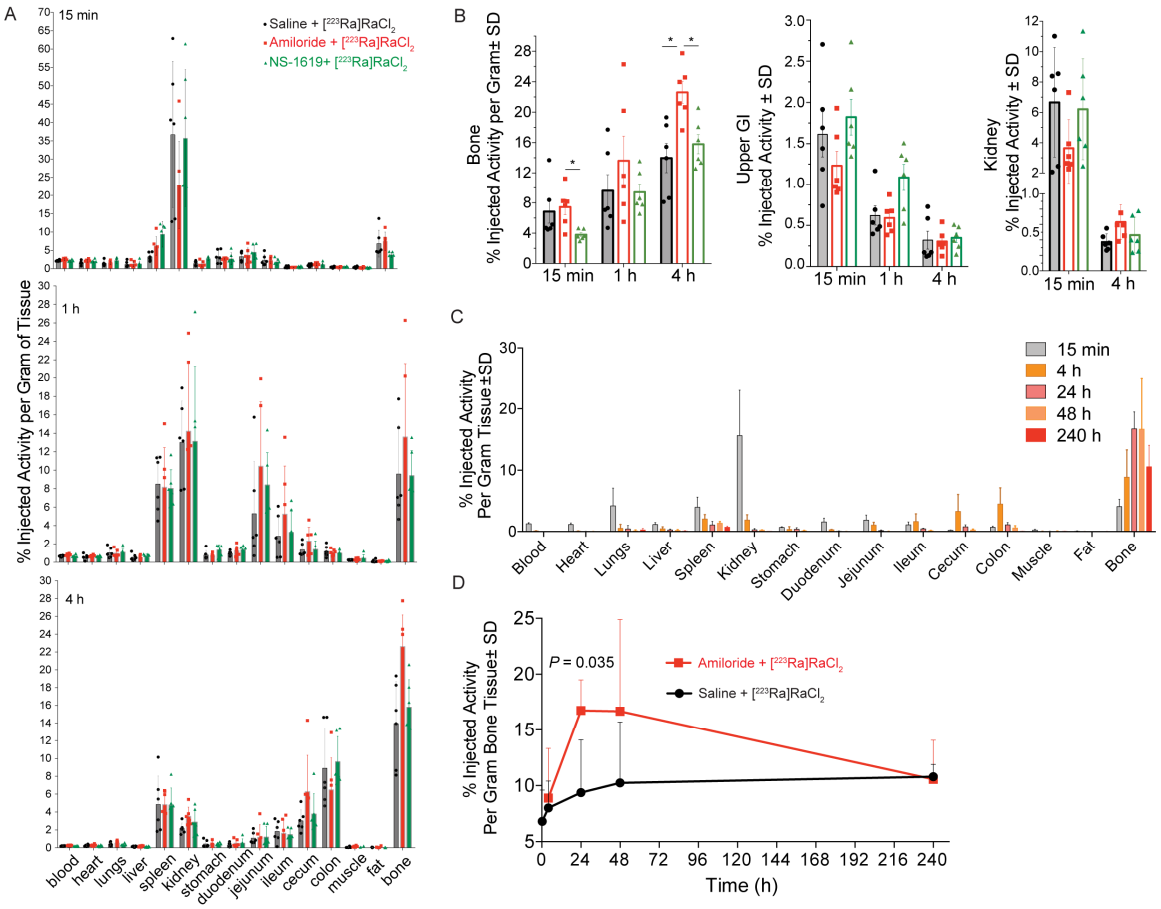

Figure 3: Evaluation of selected ion channel modulators with [^{223}Ra]$RaCl_2$; A) Radioactive organ distribution of healthy male C57Bl/6 mice randomized in 3 cohorts (n=6) given amiloride prior to [^{223}Ra]$RaCl_2$ (red); NS-1619 prior to [^{223}Ra]$RaCl_2$ (green); and saline prior to [^{223}Ra]$RaCl_2$ (grey). Several organs displayed significant differences of ^{223}Ra uptake including 1.5-fold higher bone localization with amiloride. Note differences in scale for 15 min data (values reported in Supplemental Information). B) ^{223}Ra bone activity uptake (%IA/g) at 15 min for NS-1619 combination is half that of control and amiloride-treated groups. In contrast, the amiloride-treated group shows at bone uptake significantly higher than that of control (*P<0.05). The upper GI radioactive uptake reflects higher content for NS-1619-treated animals at 15 min (*P<0.05). Kidney uptake values across the cohorts at 15 min time point shows a decreased uptake for the amiloride group. C) Whole organ distribution and D) bone-focus over 10 d time course comparing the amiloride combination to [^{223}Ra]$RaCl_2$, the activity uptake at 24 h is significantly different between the 2 groups (P=0.035).

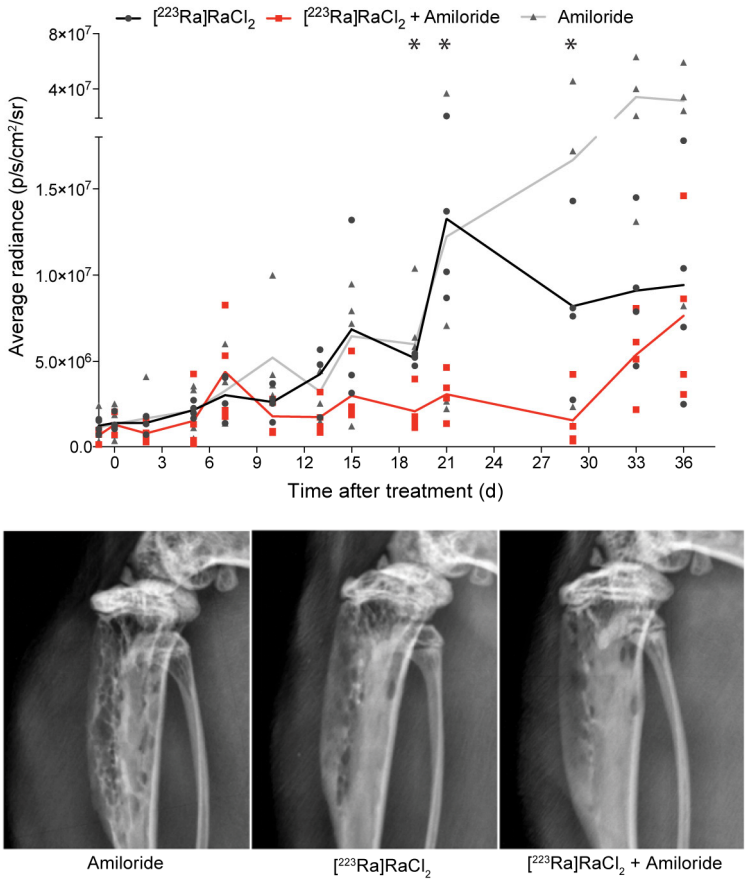

Figure 4: Tumor growth inhibition and monitoring of C4-2B bone-inoculated animals treated with: amiloride (grey); combination amiloride + [^{223}Ra]$RaCl_2$ (red) and [^{223}Ra]$RaCl_2$ alone (black). Average bioluminescent radiance measured using luciferase expressing C4-2B cells inoculated in the tibia shaft shows a superior tumor growth inhibition for the combination cohort. * indicate $P<0.05$ at day 19, 21 and 29 comparing [^{223}Ra]$RaCl_2$ with combination. Animals on the combination lost less weight, and regained that mass faster than with either agent alone (Supplemental Figure 6). Representative X-ray of tibia 35 d p.i. demonstrating degradation for the control amiloride as compared to radiotherapy and combination cohorts.

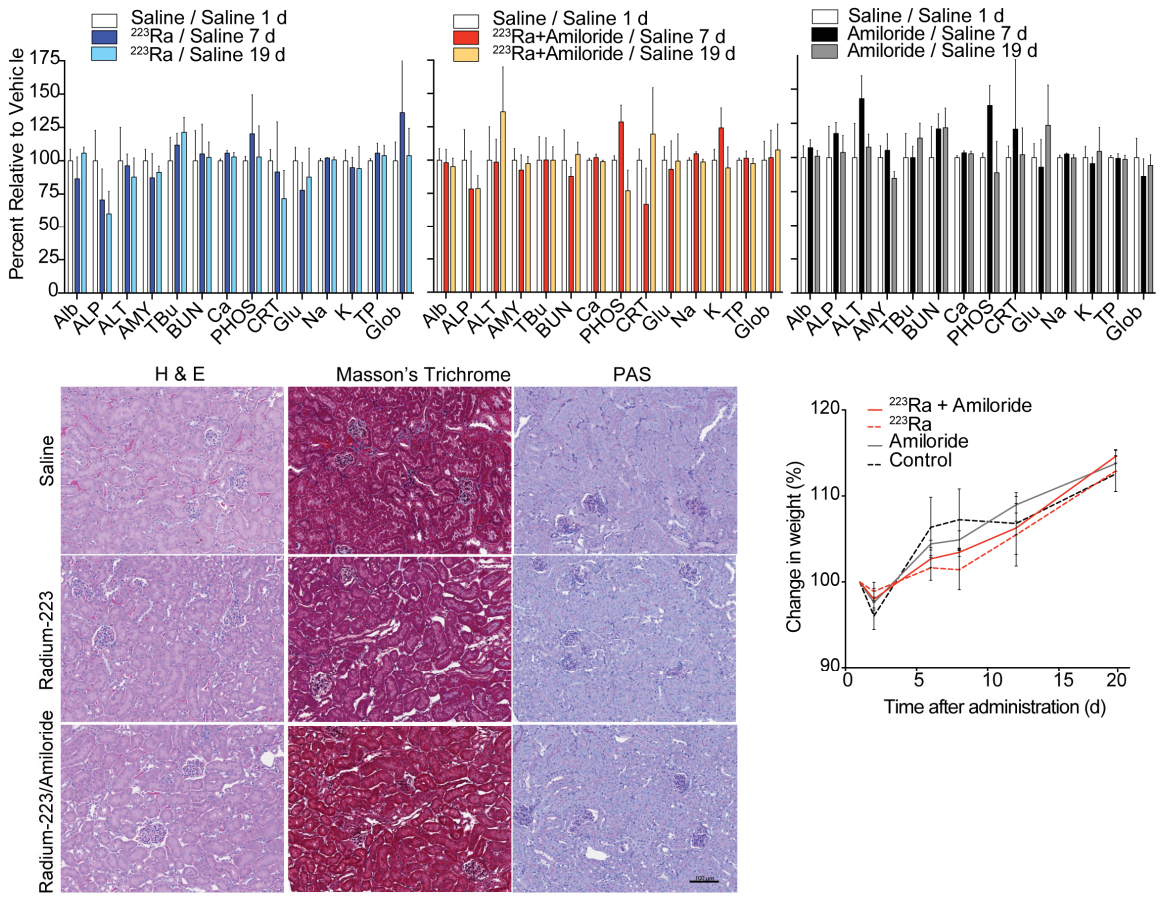

Figure 5: Toxicological Effects of Single or Combination Treatment. Blood chemistry markers for control saline, [^{223}Ra]$RaCl_2$ or amiloride alone, and the combination at 1, 7 and 19 days post administration. ALB Albumin (g/L); ALP Alkaline Phosphatase (U/L); ALT Alanine Amino Transferase (U/L); AMY Amylase (U/L); TBu Total Bilirubin (µmol/L); BUN Blood Urea Nitrogen (mmol/L); Ca Calcium (mmol/L); PHOS Phosphate (mmol/L); CRT Creatinine (µmol/L); Glu Glucose (mmol/L); Na sodium (mmol/L); K Potassium (mmol/L); TP Total Protein (g/L); Glob Globulin (g/L). For [^{223}Ra]$RaCl_2$ and combined therapy Amiloride, ALP and Creatinine present significant drop at 7 days as compared to the control saline cohort with no other noticeable differences found. Kidney pathology by hematoxylin and eosin, Masson's Trichrome, and Periodic Acid-Schiff stain at 20 days post-treatment. No morphological differences were noted. Weight monitoring demonstrated indistinguishable gain for all groups.

Graphical abstract:

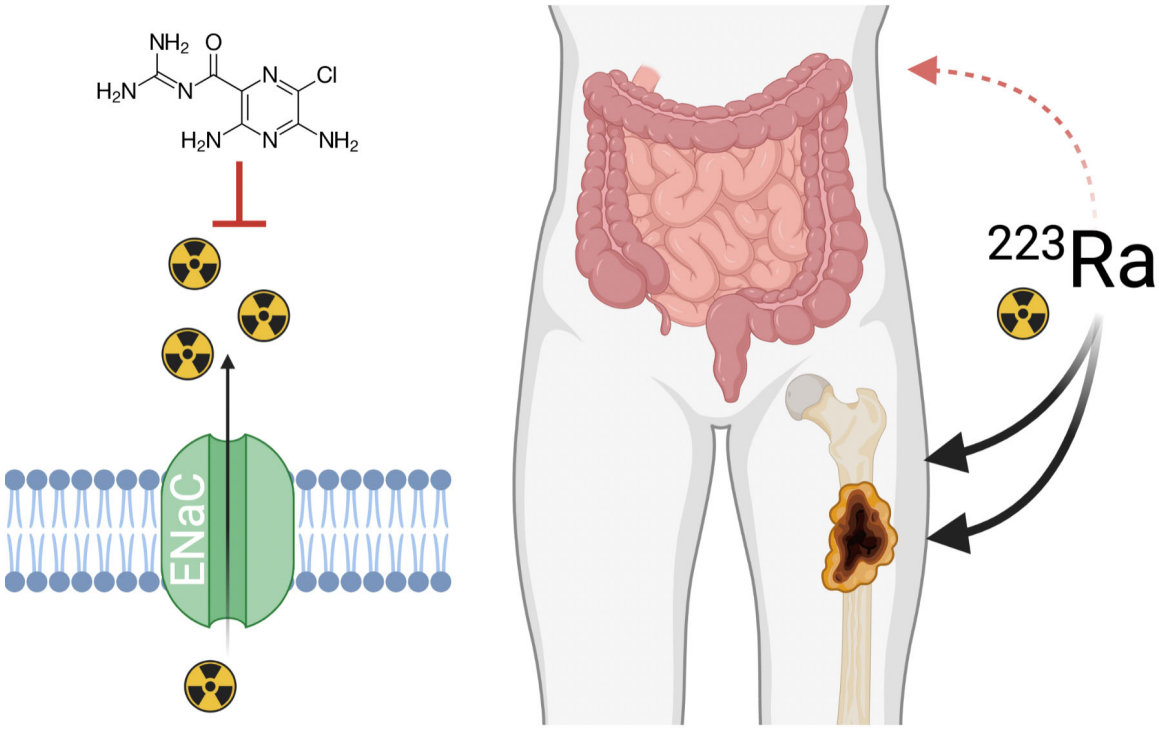

Title:

Improved Radium-223 Therapy with Combination Epithelial Sodium Channel Blockade

Supplemental Information

Authors:
Diane S. Abou[1,2,3], Amanda Fears[1], Lucy Summer[1], Mark Longtine[1], Nadia Benabdallah[1,2], Ryan C. Riddle[4,5], David Ulmert[6,7], Jeff M. Michalski[8], Richard L. Wahl[1], Denise Chesner[9], Michele Doucet[10], Nicholas C. Zachos[9], Brian W. Simons[11], Daniel L. J. Thorek[1,2,3,12]

Affiliations:
1 Mallinckrodt Institute of Radiology, Washington University in St. Louis, School of Medicine, St. Louis, Missouri, 63110
2 Program in Quantitative Molecular Therapeutics, Washington University in St. Louis, School of Medicine, St. Louis, Missouri, 63110
3 Cyclotron Facility, Washington University in St. Louis, School of Medicine, St. Louis, Missouri, 63110
4 Department of Orthopaedics, Johns Hopkins University, Baltimore, Maryland, 21205
5 Research and Development Service, Baltimore VA Medical Center, Baltimore, MD 21201
6 Department of Pharmacology, University of California Los Angeles, Los Angeles, California, 90032
7 Department of Clinical Sciences, Lund University, Barngatan 2:1, Lund, S-21185 Sweden
8 Department of Radiation Oncology, Washington University School of Medicine in St. Louis
9 Department of Medicine, Division of Gastroenterology and Hepatology, JHU School of Medicine, Baltimore, Maryland, 21225
10 Department of Oncology, JHU School of Medicine
11 Center for Comparative Medicine, Baylor College of Medicine, Houston, Texas.
12 Department of Biomedical Engineering, Washington University in St. Louis, St. Louis, Missouri, 63110

Material and Methods:

Chemicals: All the chemicals unless specified were purchased from Sigma-Aldrich. Immunohistological staining materials were purchased from Molecular Probes (Life Technologies). Goat Anti-Rabbit IgG-DyLight 680 was obtained from Thermo Scientific and mounting media DAPI or TRITC-Phalloidin from Vector Laboratories. The screen-well ion channel ligand library was acquired from Enzo Lifesciences. Microscint light scintillation cocktail was purchased from Perkin Elmer.

Isotope production and quality control: [^{223}Ra]$RaCl_2$ was produced as previously described method (*1*), pure ^{223}Ra was generated from the parent isotope ^{227}Th or ^{227}Ac source provided by Oak Ridge, Department of Energy. Briefly, 10-20 µCi of the parent isotope was adsorbed on an anionic polymeric resin Dowex 1x8 and eluted under mild acidic conditions (methanol: nitric acid (2N) 80:20) to isolate pure ^{223}Ra-nitrates. Following multiple evaporations in metal free water, the final sample was suspended in sodium citrate (0.03 M) and saline (150 mM). The radiochemical quality was checked using gamma spectrometry with a High Purity Germanium detector, showing undetectable isotopic parent breakthrough and a ^{223}Ra radiochemical purity of over 99%.

In vitro studies: To establish intestinal cellular models, we cultured human duodenal enteroids and Caco-2/BBe1 monolayers on Transwell polymeric filter plates divided into lower and upper incubation compartments, modeling the basolateral and apical side of the epithelium, respectively. This setup permitted the identification and quantification of ^{223}Ra transcellular transport, mimicking the physiological exsorption of ^{223}Ra.

Human duodenal enteroids from healthy patient-derived cellular crypts tissue samples were reconstituted and grown. Both differentiated (DF) and undifferentiated (UDF) phenotypes were tested. DF monolayers were induced by removal of Wnt3A and Rspondin-1 DFM factors from the incubation media, as described (*2*). DF cell state corresponds to villus-like cells, with higher cell heights, increased TEER and larger microvilli density as compared to UDF related to crypt-like cells. DF enteroids present higher density of NHE3 ion transporters (26% higher than UDF) and lower density of NKCC1 transport (89% less than UDF)(*3*,*4*).

DF or UDF duodenal enteroids were seeded and grown inverted (villi upward) on 6-transwell plates for 2 weeks until cell confluence was reached, leading to confluent monolayers. Monolayer integrity was checked, before and after [^{223}Ra]$RaCl_2$ incubation, by measuring surface tension TEER in Ω/m (transepithelial electrical resistance) utilizing an ohmmeter. 50 nCi (1.85 kBq) was added in the basolateral compartment and incubated at 37 °C, 5% CO_2, 1 to 24 h (n=4) before separating well for analyses. Radioactive transport was measured utilizing light scintillation counting (Topcount, PerkinElmer). Radium-223 passage was calculated as the ratio percentile of the apical sampling counts per minute (cpm) over the initial activity added; including background correction.

Caco-2/BBe1 (brush border expressing clone) monolayers were utilized for ion-channel ligand library screening (52 compounds – see Suppl. Info.) testing radioactive transfer upon epithelial ion-transport activation or blocking. Caco-2/BBe1 cells were seeded 15,000 cells per well in 96-well transwell filter plates and assayed 10 days post-seeding. The screened bioactive material was added in the basolateral well (20 µM, n=3 / molecules). 2 h following drug incubation, 3

nCi (0.1 kBq) of [^{223}Ra]$RaCl_2$ was added in the same compartment. The incubation was stopped 4 h post ^{223}Ra addition to assess radioactive transfer from basolateral to apical compartments.

The monolayer integrity was verified using lucifer yellow permeability assay. The fluorescent tracer was added in the apical compartment post-incubation, and fluorescence permeability was read sampling the basolateral media. The percent of Lucifer Yellow Passage (LYp%) was calculated as the ratio of relative Fluorescence Units-535 nm (FU) of the assayed basolateral sample over FU of a control complete transfer to the basolateral compartment (ruptured membrane). Any monolayers presenting LYp% > 1.5 were excluded from the experiment, deemed to have been damaged.

Radioactive reading was accomplished sampling the apical compartments on Luma plates and reading the dried luminescence using Topcount scintillation counter. A control assay modulator-free receiving only [^{223}Ra]$RaCl_2$, #12: control, was carried out defining the natural radioactive flux (^{223}Ra passage %) occurring through cells as the baseline value 0. Averaged (n=3) drug-assayed measurements were normalized to modulator-free flux. Results were plotted as a waterfall chart: with negative values showing ^{223}Ra blocking and positive values showing ^{223}Ra transport activation through monolayers.

List of 52 evaluated compounds in the Caco-2 monolayer screening (Figure 2)

The compounds evaluated were selected from the ion channel libarary (Screenwell, Enzo). 1: Fipronil: GABA-gated chloride-channel blocker; 2: Amiloride HCl.2H_2O: NaH channel blocker; 3: Bezamil.HCl: NaH Channel blocker; 4: AM92016: K^+ channel blocker; 5: SDZ-201 106(+/-) Na^+ channel indirect activator and K channel blocker; 6: N-phenylanthranilic acid, Cl^- channel blocker; 7: Tetrandrine: Ca^{2+} channel blocker; 8:TMB-8HCl intracellular Ca^{2+}-channel antagonist; 9: Dantrolene: Ca^{2+} channel blocker; 10 Niguldipine.HCl: Ca^{2+} channel blocker; 11: Thapsigargin: Ca^{2+} -ATPase inhibitor; 12: control saline untreated well; 13: FPL-64176: Ca^{2+} channel blocker; 14: Niflumic acid: Cl^- channel inhibitor; 15: SKF-96365: cation channel inhibitor; 16: Nitrendipine: Ca^{2+} channel blocker; 17 Procainamide.HCl: voltage-gated Na channel blocker; 18: E-4031.2HCl.2H2O: K^+ channel blocker of the hERG-type; ZM226600: K^+/ATP channel activator; 20: Aconitine: Na^+ channel activator; 21: Penitrem A: K^+-channel inhibitor; 22: Nicardipine: Ca^{2+} channel blocker; 23: PCO-400: K^+ channel activator; 24: Quinine HCl.2H_2O Ca^{2+}-activated K^+ channel blocker; 25: Amiodarone: K^+ channel inhibitor; 26: Amlodipine Ca^{2+} channel blocker; 27: Pimozide K^+ channel inhibitor; 28: 2',4'-Dichlorobenzamil.HCl: Na^+/ Ca^{2+} channel modulator; 29: Diazoxide: K^+ channel activator; 30: Verapamil. HCl: Ca^{2+} channel blocker; 31: Cyclopiazonic acid: Ca^{2+} channel modulator; 32: Gingerol: ion channel activator; Veratridine Na^+ channel activator; 34: Fluspirilene: Ca^{2+} channel blocker; 35: R-(+)IAA-94 Cl channel modulator; 36: Lidocaine.HCl.H_2O: Na^+ channel blocker; 37: Nifedipine Ca^{2+} channel blocker; 38: U-37883A ion channel blocker; 39: Flufenamic acid: ion channel modulator; 40: Phetolamine HCl: K^+/ATP channel blocker; 41: Ryanodine: intracellular Ca^{2+} channel modulator; 42: Paxilline: K^+ channel blocker; 43: 5-Hydroxydecanoic acid: Na^+/K^+ channel opener; 44: Numodipine K^+ channel blocker; 48: Propafenone: K^+ channel blocker; 49: QX-314 bromide: Na^+ channel blocker; 50: Flecainide acetate Na^+ channel blocker; 51: NS-1619: BKCa channel opener; 52: Flunarizine.2HCl: Ca^{2+} -antagonist; 53: Quinidine. HCl H2O Na^+channel blocker

In vivo studies: All animal experiments were conducted in accordance with the institutional animal care and use protocol of both the Johns Hopkins University School of Medicine and Washington University School of Medicine as well as conformed to the Guide for the Care and Use of Laboratory Animal (8^{th} Ed. National Research Council of the National Academies).

Immunohistological staining: Male C57Bl/6 mice aged 20-30 weeks old were intravenously administered with 250 kBq/kg of [^{223}Ra]$RaCl_2$. Animals were fed with Golytely (24g/350 mL) 2 h prior to injection. The study was terminated 24 h post treatment. Portions of each GI region (1 cm) duodenum, jejunum, ileum and colon were promptly harvested. GI specimens were coated with OCT and flash frozen. Transversal sectioning of GI tissues was conducted utilizing Leica 1860 microtome at 10 µm thickness. GI tissue sections were fixed by immersion in 10% paraformaldehyde (PFA) for 15 min followed by washing with Phosphate Buffered Saline 1x. Following fixation, tissues were directly mounted on slides using DAPI and/or TRITC-Phalloidin media under cover slip and imaged on a Zeiss Axioplan M1 using µmanager (version 2.0)(*6*).

For TUNEL staining, tissues were permeabilized, treated with 0.25% Triton x-100 for 15 min and washed with PBS. A second fixation using 10% PFA was performed, with slides washed with deionized water. Tissues were then subjected to buffer reaction mixtures from the Click-iT Plus TUNEL assay. Positive controls were included, with an additional DNAase treatment. Final counterstaining used Hoechst33342 (1:5000) before mounting tissue specimen under cover slip with 30% aqueous glycerol.

For γH2AX staining, tissues were fixed and underwent blocking using serum reagent, 1 h at room temperature. The primary antibody (γH2AX, rabbit antibody 1mg/mL– 1:50) was applied overnight at 4 °C in humidity chamber. Tissues were then washed and prepared for secondary antibody development using goat anti-rabbit IgG Alexa Fluor 488 (1:200) 1 h at 4 °C in humidity chamber. The resulting samples were washed, counterstained using Hoechst 3342 and mounted under cover slip with glycerol 30%.

Kidneys were collected 20 days post-treatment and the tissues were fixed in formalin for 72 h then transferred to 70% ethanol. Tissues were processed by dehydration, paraffin embedding, and sectioning at 4 µm. Adjacent sections were stained with H&E, PAS and Masson's trichrome.

Response experiments and imaging

Dosimetry: Mean absorbed radiation doses were estimated using the source and target organ framework outlined by the MIRD Committee (*7*). The mean activity of each organ at each time point (from 15 min to 10 days p.i.; Fig 3E) was used for calculations. The cumulated activity in each organ was calculated using the trapezoidal rule over the 10 days measurement. This information was entered into the program RODES (*8*,*9*). This program includes a set of anatomical mouse models. RODES computes the absorbed dose of each organ using SAF calculated for various energies of alpha particles, photons and electrons by Monte Carlo simulation using MCNPX 2.6.

Osteosarcoma murine model: Male R2G2 mice >12 wks of age (Envigo) were inoculated with 5 million SAOS2 cells in the flank and tumors grown for 100 days until mineral protuberances were detected by X-ray (Faxitron MX20). Mice were separated in 2 cohorts (n=3). We compared ^{223}Ra organ distribution with, and without, amiloride-combination treatment at 24 h post-injection. Kidney, cecum, femurs and osteosarcoma tumor tissues were collected and evaluated for gamma counting and tissue weighing %IA/g. *In vivo* whole body and post-mortem bones and osteosarcoma were imaged using x-ray to confirm the mineralization of the tumor.

Intratibial C4-2B tumor growth inhibition: 12 skeletally mature male R2G2 mice (>12 weeks old, Envigo) received intratibial inoculation of luciferase transduced C4-2B human prostate cancer cell line (*10*). 0.25 million cells were implanted in the tibia shaft. Bone tumor growths were monitored over 55 days using bioluminescent imaging with the IVIS Lumina small animal scanner (PerkinElmer). Intravenous administration of luciferin (1:1 in saline) 50 µL was conducted 2 min prior to optical imaging. Images were processed utilizing Living Image Version 4.2 software.
For treatment administration, animals were randomized in 3 cohorts (n=4), cohort (1) [^{223}Ra]$RaCl_2$; (2) [^{223}Ra]$RaCl_2$ + Amiloride; (3) Amiloride. Each group received treatments 20 days post tumor inoculation. Animals received the diuretic Amiloride dosed 12.5 mg/kg i.p. (for cohort 2 & 3) 1 h prior to [^{223}Ra]$RaCl_2$ dosed 7.4 kBq / 100 µL i.v. for cohort 1 & 2. Tumor bearing legs were monitored via bioluminescent acquisitions twice a week recording radiance normalized to values of day 0 treatment. Mice weights were recorded over the course of the experiment. The experiment was terminated 55 days post inoculation following X-rays acquisition of the disease site.

Toxicity evaluation: Healthy male mice FVB/NCR aged 14 weeks (n=5) were randomized into 4 cohorts treated with 1) [^{223}Ra]$RaCl_2$ alone (3.7 KBq/100 µL); or 2) amiloride alone (12.5 mg/kg i.p.); or 3) combination amiloride with [^{223}Ra]$RaCl_2$ or 4) control untreated (saline). The animals were maintained for 20 days following treatment with food and water and submitted to blood chemistry analysis (Abaxis Vscan 2) at day 1; 7 and 19 days. Weight was monitored for each cohort over 20 days. At the end of the study (day 20 post-treatment), animals were sacrificed and whole limbs and kidneys were harvested for gamma counting and histopathological assessments.

Dose and schedule for amiloride combination treatment: Ion channel modulators are characterized with transient activity profiled, with efficacy waning approximately 1-2 h post administration (*11*,*12*). Administered doses of the inhibitor (13 mg/kg; 26 mg/kg) and different times of amiloride administration (15 min, 1 h, 3 h) prior to [^{223}Ra]$RaCl_2$ were tested to comparatively evaluate ^{223}Ra distribution. Organs were harvested at 24 h following [^{223}Ra]$RaCl_2$ administration. The organs distribution data are shown in Supplemental Figure 3 and 4. No significant differences were found in organ distribution whether changing doses or time of amiloride injections relative to [^{223}Ra]$RaCl_2$. For all other amiloride combination studies, 12.5-13mg/kg amiloride dosage and i.p. injection 1 h prior [^{223}Ra]$RaCl_2$ were the chosen parameters.

Statistics: All P-values were calculated with unpaired two-tailed t-test with equal Standard Deviation (SD), utilizing Graphpad, Prism software (version 6D). Significant differences were expressed at $P<0.05$ and $P<0.1$ for *in vitro* (n>4) and *in vivo* experiments (n>6).

SUPPLEMENTAL FIGURES:

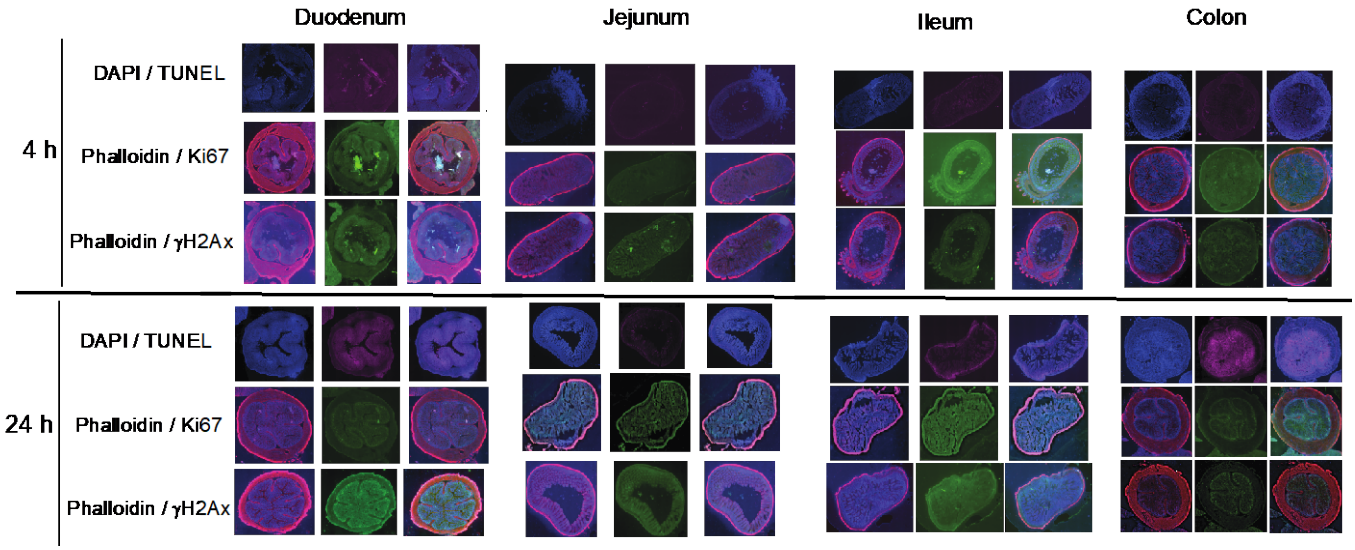

Supplemental Figure 1: Immunofluorescence by DAPI, TUNEL, Ki67 and γH_2AX of duodenum, jejunum, ileum and colon tissue sections following [^{223}Ra]$RaCl_2$ administration. Tissues were harvested at 4 (upper panels) and 24 h (lower panels) post-^{223}Ra injection.

For each organ panel, the first line displays DAPI and TUNEL staining: with upper left corner DAPI in blue displaying cell nuclei and middle slide presenting TUNEL in purple and overlaid with DAPI in the right; the second line shows Phalloidin and Ki67: middle left displays phalloidin (red + blue) staining cytoskeletal structures; middle and right corner slides present Ki67, marker of cell proliferation, in green and overlaid with phalloidin in the right; the third line shows Phalloidin and γH_2AX: phalloidin (red + blue in the left corner), the lower middle slide presents γH_2AX (green) recognizing DNA damage and overlay with phalloidin (far rights). Of all organs and time points, only duodenum and colon at 24 h post-^{223}Ra administration presented both γ-H2AX and TUNEL positive staining following ^{223}Ra alpha emission related damages.

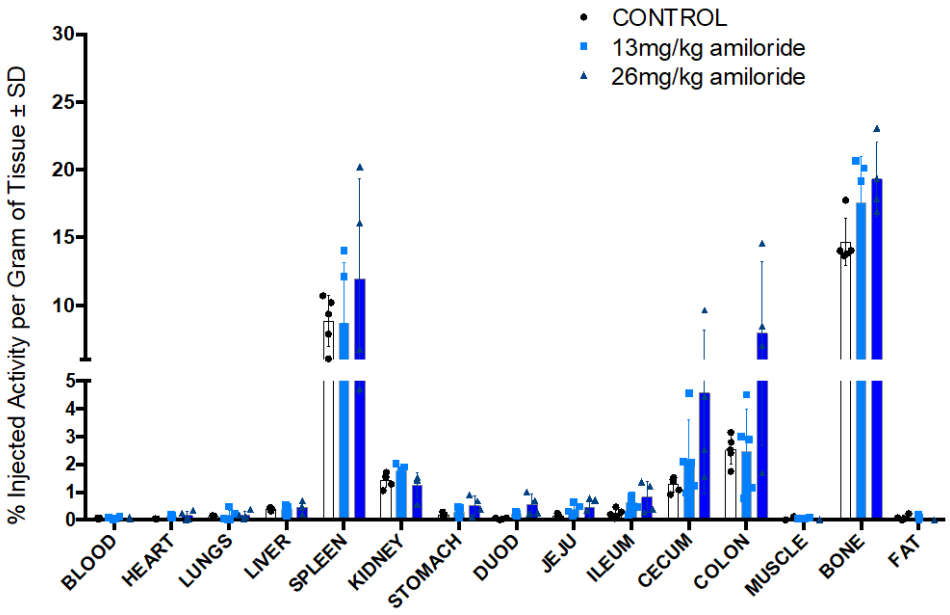

Supplemental Figure 2: Dosing optimization of amiloride comparing the radioactive organ distribution at 24 h p.i. with 13 mg/kg and 26 mg/kg administered intraperitoneally 1 h prior combination with [^{223}Ra]$RaCl_2$, administered intraveneously.

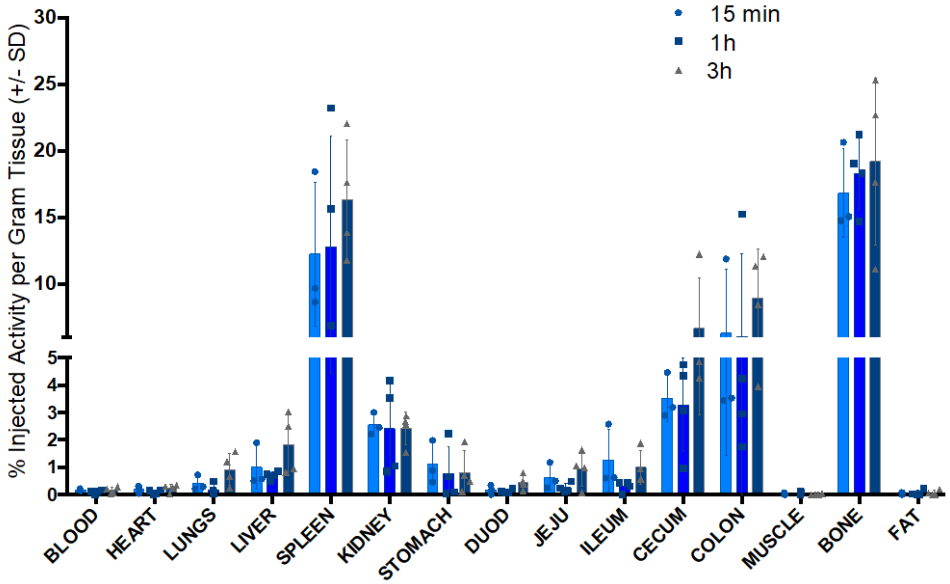

Supplemental Figure 3: Timing optimization of amiloride injection (intraperitoneal) at 13 mg/kg combined with [^{223}Ra]$RaCl_2$ (intraveneously) conducted comparing whole organ distribution collected at 24 h post radioactive administration.

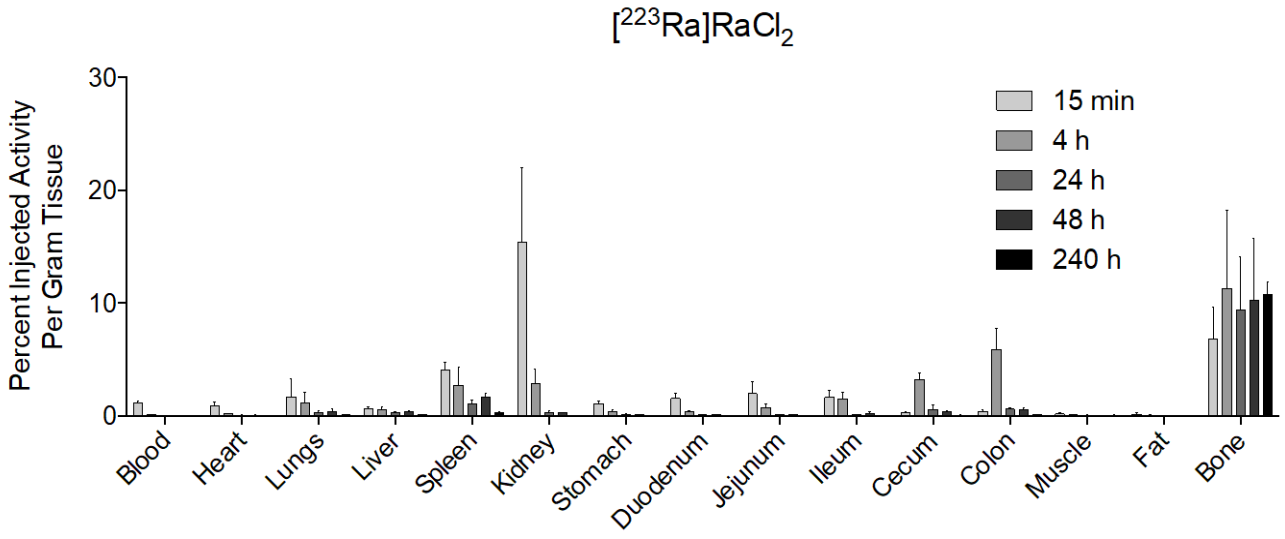

Supplemental Figure 4: [^{223}Ra]RaCl$_2$ organ distribution (%IA/g) in healthy skeletally mature mice Bl6/C57 (aged >10 weeks) from 15 min to 10 days

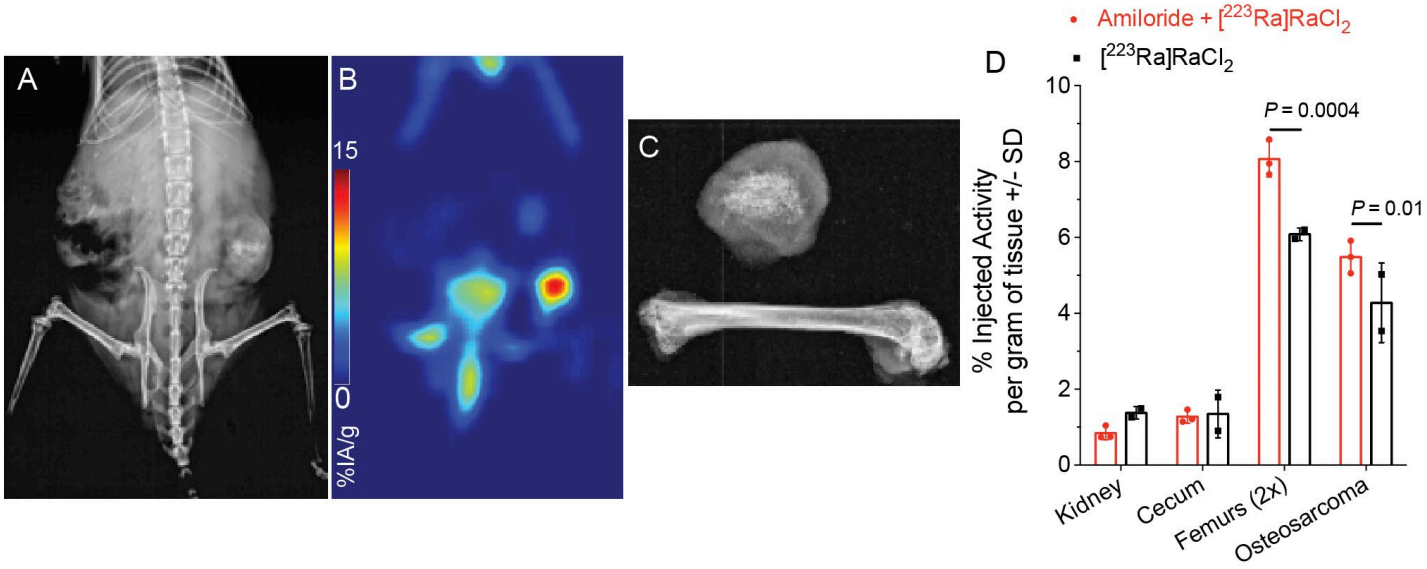

Supplemental Figure 5: Effect of amiloride on Radium-223 Uptake in Osteosarcoma Xenograft: A) Whole-body X-ray images of mice bearing flank SAOS2 xenografts; B) Whole-body [^{18}F]NaF PET scan of osseous tissue, at day of treatment. C) *Ex vivo* radiographs of extracted diseased mineral tissues and femur. D) Tissue uptake 24 h post-administration comparing combination amiloride to saline with [^{223}Ra]RaCl$_2$. No difference in renal or gut uptake was noted. Increased ^{223}Ra uptake in long bones and in the pathological osseous sites were observed for the combination ENaC treated group.

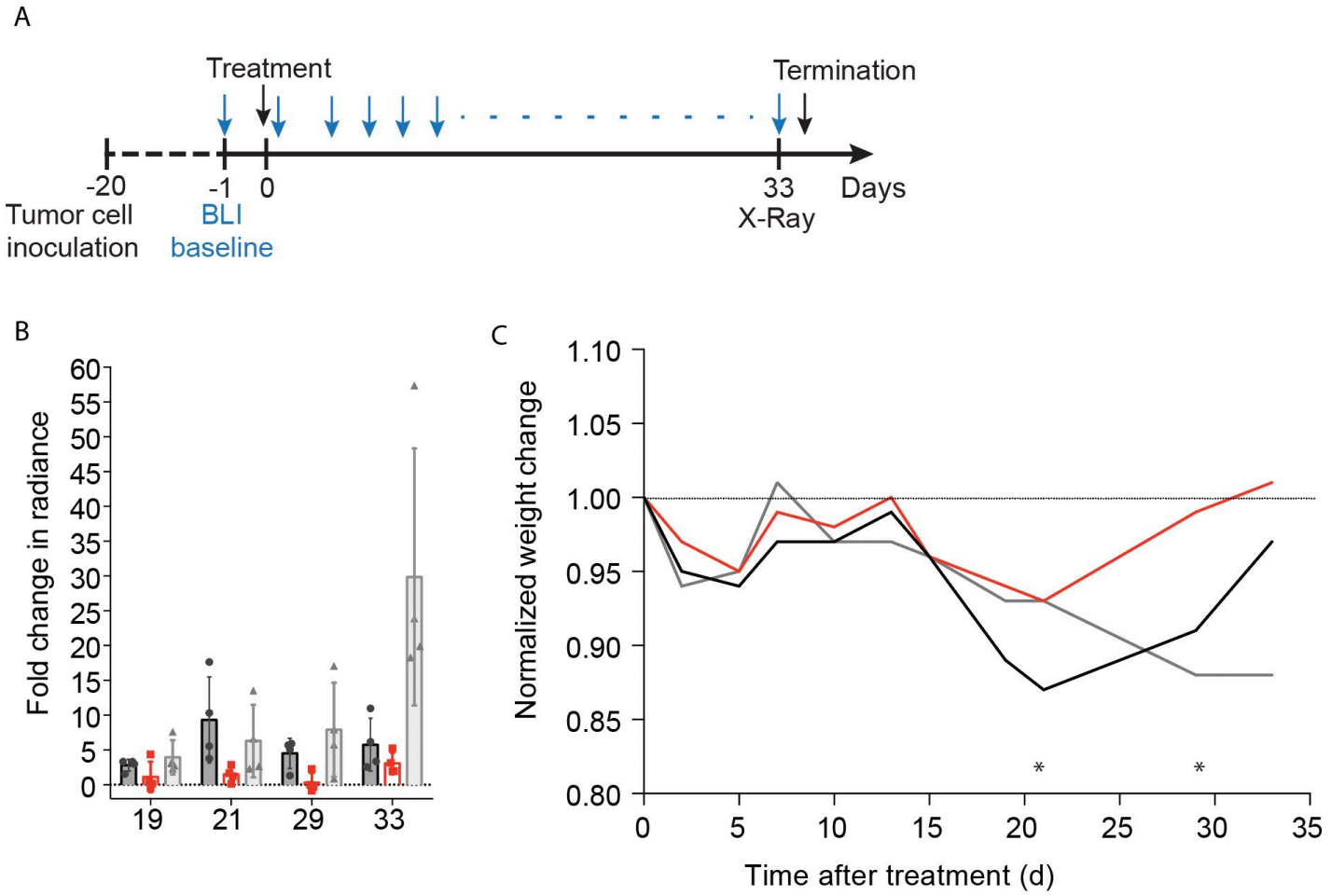

Supplemental Figure 6: A) Cells (C4-2B) were inoculated in the tibia shaft 20 days prior treatments. Animals were monitored over 35 days with indicated imaging and treatment from tumor inoculation to termination. B) Fold change of tumor radiance normalized to that of treatment day. C) Mice average normalized weight showing regain of weight for the combination cohort in contrast to the 2 other groups failing to return to initial weight. * indicates $P \leq 0.05$ at day 21 and 29 comparing [^{223}Ra]$RaCl_2$ with combination.

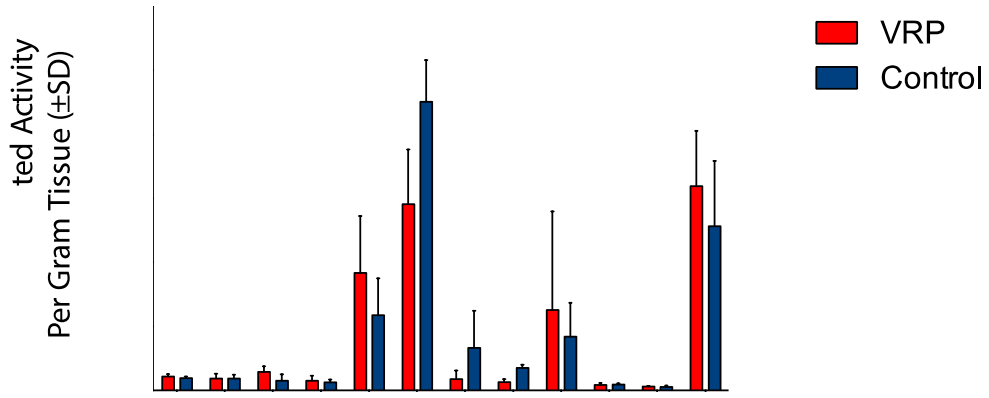

Supplemental Figure 7: ^{223}Ra organ distribution 1 h post [^{223}Ra]$RaCl_2$ administration, comparing the combination verapamil (VRP) (Ca^{2+} channel blocker) with [^{223}Ra]$RaCl_2$. Animals were administered VRP intraperitoneally 1 h prior radiopharmaceutical administration. None of the organs except the cecum presented any statistical differences considering *P* values (student's T test).

SUPPLEMENTAL TABLES:

	Saline + Radium-223			Amiloride + Radium-223			NS-1619 + Radium-223		
%IA	15 min (n=6)	1h (n=6)	4h (n=6)	15 min (n=6)	1h (n=6)	4h (n=6)	15 min (n=6)	1h (n=6)	4h (n=6)
Blood	0.66 ± 0.14	0.21 ± 0.04	0.07 ± 0.02	0.82 ± 0.12	0.23 ± 0.04	0.08 ± 0.02	0.72 ± 0.16	0.22 ± 0.05	0.07 ± 0.02
Heart	0.30 ± 0.09	0.13 ± 0.03	0.05 ± 0.02	0.38 ± 0.07	0.12 ± 0.02	0.05 ± 0.03	0.42 ± 0.08	0.11 ± 0.02	0.04 ± 0.02
Lungs	0.31 ± 0.16	0.21 ± 0.09	0.09 ± 0.04	0.33 ± 0.09	0.23 ± 0.11	0.12 ± 0.05	0.47 ± 0.19	0.22 ± 0.10	0.07 ± 0.02
Liver	1.01 ± 0.55	0.51 ± 0.30	0.12 ± 0.06	1.07 ± 0.59	0.42 ± 0.20	0.13 ± 0.06	1.01 ± 0.42	0.52 ± 0.14	0.10 ± 0.05
Spleen	0.28 ± 0.06	0.73 ± 0.32	0.36 ± 0.25	0.40 ± 0.15	0.56 ± 0.21	0.35 ± 0.12	0.72 ± 0.25	0.57 ± 0.17	0.37 ± 0.14
Kidney	6.66 ± 3.29	2.39 ± 0.79	0.37 ± 0.10	3.64 ± 1.72	2.40 ± 1.05	0.63 ± 0.21	6.21 ± 3.04	2.20 ± 1.15	0.46 ± 0.21
Stomach	0.94 ± 0.47	0.44 ± 0.22	0.27 ± 0.20	0.78 ± 0.40	0.38 ± 0.08	0.22 ± 0.14	1.33 ± 0.21	0.83 ± 0.39	0.26 ± 0.10
Duodenum	0.68 ± 0.39	0.18 ± 0.06	0.05 ± 0.04	0.45 ± 0.07	0.21 ± 0.10	0.08 ± 0.07	0.50 ± 0.29	0.26 ± 0.08	0.09 ± 0.09
Ileum	0.58 ± 0.38	0.95 ± 1.02	0.12 ± 0.09	0.51 ± 0.29	1.75 ± 1.29	0.19 ± 0.26	0.78 ± 0.40	1.52 ± 0.60	0.21 ± 0.21
Jejunum	0.33 ± 0.18	0.34 ± 0.28	0.24 ± 0.16	0.31 ± 0.12	0.57 ± 0.55	0.17 ± 0.17	0.26 ± 0.12	0.42 ± 0.31	0.18 ± 0.08
Cecum	0.23 ± 0.17	0.77 ± 0.35	1.52 ± 0.48	0.19 ± 0.03	1.01 ± 0.54	2.67 ± 1.17	0.27 ± 0.10	0.70 ± 0.50	2.01 ± 1.22
Colon	0.17 ± 0.05	0.20 ± 0.09	1.96 ± 0.83	0.19 ± 0.03	0.20 ± 0.06	1.45 ± 0.80	0.18 ± 0.02	0.17 ± 0.04	2.33 ± 0.65
Muscle	0.05 ± 0.03	0.04 ± 0.01	0.01 ± 0.01	0.05 ± 0.02	0.03 ± 0.02	0.02 ± 0.01	0.06 ± 0.02	0.05 ± 0.04	0.00 ± 0.01
Fat	0.05 ± 0.03	0.01 ± 0.01	0.00 ± 0.00	0.04 ± 0.04	0.01 ± 0.01	0.01 ± 0.01	0.03 ± 0.02	0.02 ± 0.01	0.00 ± 0.00
Bone	0.59 ± 0.17	0.69 ± 0.30	1.19 ± 0.24	0.59 ± 0.29	0.88 ± 0.35	1.83 ± 0.30	0.33 ± 0.11	0.67 ± 0.14	1.17 ± 0.16

	Saline + Radium-223			Amiloride + Radium-223			NS-1619 + Radium-223		
%IA/g	15 min (n=6)	1h (n=6)	4h (n=6)	15 min (n=6)	1h (n=6)	4h (n=6)	15 min (n=6)	1h (n=6)	4h (n=6)
Blood	2.17 ± 0.19	0.65 ± 0.08	0.20 ± 0.03	2.47 ± 0.27	0.77 ± 0.13	0.26 ± 0.03	2.08 ± 0.30	0.65 ± 0.12	0.18 ± 0.04
Heart	1.56 ± 0.50	0.56 ± 0.27	0.24 ± 0.10	2.12 ± 0.34	0.66 ± 0.10	0.27 ± 0.10	2.04 ± 0.39	0.60 ± 0.08	0.20 ± 0.08
Lungs	1.44 ± 0.66	1.03 ± 0.52	0.42 ± 0.19	1.57 ± 0.45	0.96 ± 0.39	0.53 ± 0.23	2.21 ± 0.76	1.07 ± 0.41	0.35 ± 0.11
Liver	1.15 ± 0.74	0.52 ± 0.33	0.14 ± 0.06	1.29 ± 0.71	0.46 ± 0.21	0.16 ± 0.07	1.30 ± 0.74	0.66 ± 0.19	0.11 ± 0.06
Spleen	3.24 ± 1.02	8.51 ± 2.80	4.85 ± 2.92	6.19 ± 2.34	8.16 ± 3.91	4.81 ± 1.52	9.38 ± 3.20	8.04 ± 1.85	4.77 ± 1.75
Kidney	36.68 ± 18.28	13.01 ± 4.09	2.17 ± 0.55	22.92 ± 10.99	14.22 ± 6.94	3.50 ± 0.95	35.70 ± 17.07	13.11 ± 7.44	2.87 ± 1.34
Stomach	1.39 ± 0.60	0.76 ± 0.47	0.44 ± 0.37	1.28 ± 0.72	0.67 ± 0.23	0.40 ± 0.25	2.73 ± 0.44	1.32 ± 0.55	0.40 ± 0.15
Duodenum	3.27 ± 1.62	0.96 ± 0.24	0.32 ± 0.23	2.61 ± 0.26	1.24 ± 0.50	0.51 ± 0.37	2.69 ± 1.51	1.34 ± 0.42	0.51 ± 0.45
Ileum	3.27 ± 1.25	5.30 ± 5.17	1.08 ± 0.61	3.59 ± 1.91	10.43 ± 6.37	1.18 ± 1.29	4.47 ± 1.81	8.41 ± 3.19	1.20 ± 1.09
Jejunum	2.33 ± 1.35	2.86 ± 2.11	1.83 ± 1.09	2.24 ± 0.80	5.25 ± 4.74	1.61 ± 1.41	1.88 ± 0.81	3.27 ± 2.26	1.48 ± 0.57
Cecum	0.43 ± 0.27	1.35 ± 0.65	3.02 ± 1.12	0.37 ± 0.04	2.32 ± 1.37	6.28 ± 3.73	0.50 ± 0.19	1.39 ± 0.88	3.77 ± 2.10
Colon	0.97 ± 0.31	1.17 ± 0.56	8.91 ± 4.16	1.18 ± 0.36	1.07 ± 0.32	6.49 ± 3.28	1.13 ± 0.48	0.96 ± 0.27	9.62 ± 2.62
Muscle	0.41 ± 0.18	0.25 ± 0.01	0.06 ± 0.06	0.37 ± 0.12	0.28 ± 0.14	0.14 ± 0.07	0.46 ± 0.13	0.41 ± 0.38	0.03 ± 0.08
Fat	0.36 ± 0.22	0.12 ± 0.14	0.04 ± 0.03	0.26 ± 0.16	0.09 ± 0.04	0.05 ± 0.09	0.25 ± 0.12	0.11 ± 0.08	0.01 ± 0.02
Bone	6.83 ± 3.35	9.60 ± 4.80	13.96 ± 4.32	7.45 ± 2.31	13.60 ± 7.29	22.62 ± 3.24	3.80 ± 0.62	9.41 ± 2.48	15.79 ± 2.84

%IA/g P values 15 m - Bones	Radium	Radium+Amiloride	Radium+NS1619
Radium+NS1619	0.0742	**0.0066**	_
Radium+Amiloride	0.7412	_	
Radium	_		
P values 1 h - Bones			
Radium+NS1619	0.9399	0.2516	_
Radium+Amiloride	0.3291	_	
Radium	_		
P values 4 h - Bones			
Radium+NS1619	0.4465	**0.0054**	_
Radium+Amiloride	**0.005**	_	
Radium	_		

%IA P values 15 m - Kidneys	Radium	Radium+Amiloride	Radium+NS1619
Radium+NS1619	0.8272	0.1307	_
Radium+Amiloride	0.0994	_	
Radium	_		
%IA P values 4 h - Kidneys			
Radium+NS1619	0.4092	0.2317	_
Radium+Amiloride	**0.0305**	_	
Radium	_		

%IA P values 15 m - UpperGI	Radium	Radium+Amiloride	Radium+NS1619
Radium+NS1619	0.5648	0.059	_
Radium+Amiloride	0.2663	_	
Radium	_		
P values 1 h - UpperGI			
Radium+NS1619	**0.0403**	**0.0185**	_
Radium+Amiloride	0.8303	_	
Radium	_		
P values 4 h - UpperGI			
Radium+NS1619	0.8207	0.6037	_
Radium+Amiloride	0.9057	_	
Radium	_		

%IA P values 15 m - Spleen	Radium	Radium+Amiloride	Radium+NS1619
Radium+NS1619	**0.0027**	**0.0325**	_
Radium+Amiloride	0.112	_	
Radium	_		

Supplemental Table 1: Numerical values % Injected Activity (IA) and % IA/gram (n=6) and statistics using the student t-test P values of ^{223}Ra whole organ distribution presented in Figure 2A comparing [^{223}Ra]$RaCl_2$; with Amiloride + [^{223}Ra]$RaCl_2$ and NS-1619 + [^{223}Ra]$RaCl_2$ at 15 min, 1 h and 4 h post [^{223}Ra]$RaCl_2$ administration

	15 min			4 h			24 h			48 h			240 h		
Combination	Mean (%IA/g)	SD	n	Mean (%IA/g)	SD	n	Mean (%IA/g)	SD	n	Mean (%IA/g)	SD	n	Mean (%IA/g)	SD	n
Blood	1.286136	0.1680353	4	0.1263299	0.02707957	4	0.02791498	0.00706568	4	0.007460109	0.00412874	4	0.02205042	0.00980587	4
Heart	1.157887	0.2626306	4	0.1136984	0.01952666	4	0.0451764	0.0302837	4	0.0387573	0.01660495	4	0.02262329	0.01746565	4
Lungs	4.213633	2.863407	4	0.5598086	0.615557	4	0.4293593	0.5592576	4	0.1448156	0.1761845	4	0.2928722	0.2434169	4
Liver	1.174585	0.3116064	4	0.4847367	0.3016431	4	0.2809911	0.1473182	4	0.202307	0.1724876	4	0.1054092	0.08302517	4
Spleen	3.980962	1.649713	4	2.091122	0.7017254	4	1.076818	0.6191714	4	1.379065	0.2882899	4	0.7410591	0.1591555	4
Kidney	15.64385	7.404927	4	1.901285	0.8503923	4	0.3228253	0.1848896	4	0.2558807	0.05419715	4	0.08307688	0.01423772	4
Stomach	0.6877006	0.1149299	4	0.3753085	0.4441946	4	0.4243939	0.2457922	4	0.1675111	0.07751615	4	0.03871745	0.02140627	4
Duodenum	1.583079	0.6404865	4	0.3430845	0.04867064	4	0.09636526	0.03002037	4	0.04478013	0.02044326	4	0.03218402	0.02918036	4
Jejunum	1.886994	0.8238677	4	1.089947	0.444753	4	0.1811629	0.1052425	4	0.07035638	0.0280624	4	0.02390192	0.01156451	4
Ileum	1.100085	0.4817129	4	1.670939	1.23118	4	0.4504758	0.1035889	4	0.1660643	0.06758376	4	0.02209063	0.01136822	4
Cecum	0.2365118	0.05015518	4	3.305635	2.760669	4	0.7955292	0.3130657	4	0.2945002	0.1428603	4	0.0448446	0.01899982	4
Colon	0.7195342	0.1887262	4	4.506662	2.624808	4	1.106817	0.3928619	4	0.6158786	0.3374675	4	0.07782671	0.02325246	4
Muscle	0.2653613	0.1414104	4	0.05186733	0.0243437	4	0.0563924	0.06485684	4	0.06191725	0.0748892	4	0.07579432	0.04400966	4
Fat	0.09526733	0.04822477	4	0.02147359	0.0195352	4	0.007696052	0.00474124	4	0.001670262	0.01081174	4	0.05655225	0.02224042	4
Bone	4.097728	1.15579	4	8.885285	4.436336	4	16.74254	2.742961	4	16.67759	8.223642	4	10.56088	3.498785	4

	15 min			4 h			24 h			48 h			240 h		
[^{223}Ra]RaCl$_2$	Mean (%IA/g)	SD	n	Mean (%IA/g)	SD	n	Mean (%IA/g)	SD	n	Mean (%IA/g)	SD	n	Mean (%IA/g)	SD	n
Blood	1.169538	0.09391656	4	0.1175373	0.01401238	4	0.01734663	0.01077043	4	0.01505588	0.00464882	4	0.006340256	0.00406584	4
Heart	0.8432367	0.3732072	4	0.1532283	0.03274979	4	0.04057152	0.02742222	4	0.04119933	0.01166959	4	0.004382428	0.02268926	4
Lungs	1.682146	1.603887	4	1.130225	0.9612913	4	0.2313552	0.2633644	4	0.3409219	0.3254534	4	0.0578289	0.02354648	4
Liver	0.6280642	0.1558409	4	0.5203158	0.2788523	4	0.2591377	0.09680536	4	0.3389141	0.09255996	4	0.06476675	0.05741169	4
Spleen	4.089929	0.6840701	4	2.69554	1.557598	4	1.022419	0.3719779	4	1.636318	0.4054865	4	0.2882278	0.07591362	4
Kidney	15.38772	6.590871	4	2.828296	1.3013	4	0.2426343	0.1712796	4	0.2571676	0.0669317	4	0.04087569	0.00774256	4
Stomach	1.05076	0.2781586	4	0.3717034	0.1899036	4	0.124045	0.09203762	4	0.08414359	0.02250614	4	0.02125757	0.01147008	4
Duodenum	1.542569	0.504703	4	0.3408047	0.1088364	4	0.05678289	0.02361137	4	0.05606991	0.01328332	4	0.01675255	0.02078001	4
Jejunum	1.971558	1.004884	4	0.7009393	0.3130281	4	0.05096411	0.03533968	4	0.07919758	0.04484299	4	0.02081099	0.01346771	4
Ileum	1.641311	0.606918	4	1.487142	0.618979	4	0.0956083	0.02512994	4	0.2067748	0.1281618	4	0.03235535	0.00867425	4
Cecum	0.2738736	0.08864974	4	3.213955	0.5493559	4	0.5723614	0.4190339	4	0.3357381	0.08162646	4	0.03556774	0.01519967	4
Colon	0.3963575	0.1525496	4	5.880912	1.86738	4	0.586316	0.1284722	4	0.56862	0.1622569	4	0.06540006	0.02410631	4
Muscle	0.1656154	0.07440572	4	0.0640504	0.0772082	4	0.008208609	0.04498434	4	0.004148945	0.01037712	4	0.02768566	0.0279186	4
Fat	0.1336298	0.1099008	4	0.03355403	0.02639345	4	-0.01560238	0.02921376	4	0.000824541	0.0160607	4	0.00505117	0.01669823	4
Bone	6.806796	2.809202	4	11.31279	6.884089	4	9.375665	4.733264	4	10.24459	5.484949	4	10.78348	1.114516	4

Supplemental Table 2: Mean % Injected Activity per gram (%IA/g) ± SD (Standard Deviation) values of ^{223}Ra organ distribution (n=4 / group) of amiloride combination versus [^{223}Ra]RaCl$_2$ administered mice acquired from 15 min to10 days (values plotted in Figure 3E and Fig. s3).

Absorbed Dose (Gy)	Heart	Lungs	Liver	Spleen	Kidneys	Stomach	Intestine	Skeleton
Combination	0.01	0.04	0.01	0.12	0.02	0.03	0.02	1.43
[^{223}Ra]RaCl$_2$	0.01	0.04	0.01	0.13	0.02	0.02	0.03	1.07

Supplemental Table 3: Comparative organ dosimetry of combination Amiloride / [^{223}Ra]RaCl$_2$ with [^{223}Ra]RaCl$_2$ over 10 days

Supplemental References:

1. Abou DS, Pickett J, Mattson JE, Thorek DLJ. A Radium-223 microgenerator from cyclotron-produced trace Actinium-227. *Appl Radiat Isot*. 2017;119:36-42.

2. Noel G, Baetz NW, Staab JF, et al. A primary human macrophage-enteroid co-culture model to investigate mucosal gut physiology and host-pathogen interactions. *Sci Rep*. 2017;7:45270.

3. Foulke-Abel J, In J, Yin J, et al. Human enteroids as a model of upper small intestinal ion transport physiology and pathophysiology. *Gastroenterology*. 2016;150:638-649.e8.

4. Foulke-Abel J, In J, Kovbasnjuk O, Zachos NC. Human intestinal enteroids: a new model to study human rotavirus infection, host restriction and pathophysiology. *Journal of*. 2015.

5. Schindelin J, Arganda-Carreras I, Frise E, et al. Fiji: an open-source platform for biological-image analysis. *Nat Methods*. 2012;9:676-682.

6. Edelstein AD, Tsuchida MA, Amodaj N, Pinkard H, Vale RD, Stuurman N. Advanced methods of microscope control using μManager software. *J Biol Methods*. 2014;1:10.

7. Bolch WE, Eckerman KF, Sgouros G, Thomas SR. MIRD Pamphlet No. 21: A Generalized Schema for Radiopharmaceutical Dosimetry—Standardization of Nomenclature. *J Nucl Med*. 2009;50:477-484.

8. Miloudi H, Locatelli M, Autret G, et al. Application of rodes software to experimental biokinetic data for dose assessment in mice and rats. *J Radiol Prot*. 2017;37:564-583.

9. Locatelli M, Miloudi H, Autret G, et al. RODES software for dose assessment of rats and mice contaminated with radionuclides. *J Radiol Prot*. 2017;37:214-229.

10. Dondossola E, Casarin S, Paindelli C, et al. Radium 223-mediated zonal cytotoxicity of prostate cancer in bone. *J Natl Cancer Inst*. January 2019.

11. Ningaraj NS, Rao M, Hashizume K, Asotra K, Black KL. Regulation of blood-brain tumor barrier permeability by calcium-activated potassium channels. *J Pharmacol Exp Ther*. 2002;301:838-851.

12. Vidt DG. Mechanism of action, pharmacokinetics, adverse effects, and therapeutic uses of amiloride hydrochloride, a new potassium-sparing diuretic. *Pharmacotherapy*. 1981;1:179-187.